CRREL REPORT 96-14

Material Testing and Initial Pavement Design Modeling

Minnesota Road Research Project

Susan R. Bigl and Richard L. Berg

September 1996

Abstract: Between January 1990 and December 1994, a study verified and applied a Corps of Engineers-developed mechanistic design and evaluation method for pavements in seasonal frost areas as part of a Construction Productivity Advancement Research (CPAR) project between the Minnesota Department of Transportation (Mn/DOT) and the U.S. Army Cold Regions Research and Engineering Laboratory (CRREL). The study involved four primary components. Mn/DOT constructed a full scale pavement test facility adjacent to Interstate 94, referred to as the Minnesota Road Research Project (Mn/ROAD). CRREL performed extensive laboratory tests on the base and subgrade materials from Mn/ROAD to characterize them and their behavior under seasonal frost conditions. Laboratory tests provided the input parameters necessary for the study's third component, modeling with the CRREL Mechanistic Pavement Design and Evaluation Procedure. The modeling effort was conducted in three phases, which investigated the effects of freeze season characteristics, water table position, asphalt model and subgrade characteristics on the predicted performance of selected Mn/ROAD test sections. Delays in construction on the Mn/ROAD facility prevented the completion of the study's fourth component—using performance data from Mn/ROAD to validate the mechanistic pavement design and evaluation procedure. The report details results from the other three components.

Cover: Aerial view of Minnesota Road Research Project (Mn/ROAD).

How to get copies of CRREL technical publications:

Department of Defense personnel and contractors may order reports through the Defense Technical Information Center:
DTIC-BR SUITE 0944
8725 JOHN J KINGMAN RD
FT BELVOIR VA 22060-6218
Telephone 1 800 225 3842
E-mail help@dtic.mil
msorders@dtic.mil
WWW http://www.dtic.dla.mil/

All others may order reports through the National Technical Information Service:
NTIS
5285 PORT ROYAL RD
SPRINGFIELD VA 22161
Telephone 1 703 487 4650
1 703 487 4639 (TDD for the hearing-impaired)
E-mail orders@ntis.fedworld.gov
WWW http://www.fedworld.gov/ntis/ntishome.html

A complete list of all CRREL technical publications is available from:
USACRREL (CECRL-TL)
72 LYME RD
HANOVER NH 03755-1290
Telephone 1 603 646 4338
E-mail techpubs@crrel.usace.army.mil

For information on all aspects of the Cold Regions Research and Engineering Laboratory, visit our World Wide Web site:
http://www.crrel.usace.army.mil

CRREL Report 96-14

US Army Corps of Engineers
Cold Regions Research & Engineering Laboratory

Material Testing and Initial Pavement Design Modeling

Minnesota Road Research Project

Susan R. Bigl and Richard L. Berg

September 1996

Prepared for
MINNESOTA DEPARTMENT OF TRANSPORTATION

PREFACE

This report was prepared by Susan R. Bigl, Research Physical Scientist, Civil and Geotechnical Research Division, Research and Engineering Directorate, U.S. Army Cold Regions Research and Engineering Laboratory (CRREL), Hanover, New Hampshire, and by Dr. Richard L. Berg, formerly a Research Civil Engineer at CRREL.

This work was funded through Agreement 64632, Task Order 1 with the Minnesota Department of Transportation (Mn/DOT) and a Construction Productivity Advancement Research (CPAR) project between Mn/DOT and CRREL.

The authors thank George Cochran of the Minnesota Road Research Project and Dr. Vincent Janoo of CRREL for technically reviewing the manuscript of this report.

The soils testing information reported here is the result of work done by a team of personnel who work in the Soils Laboratory at CRREL. Their efforts are greatly appreciated. Jeffrey Stark, Soils Laboratory Manager, coordinated and initiated the work, and designed some new devices to aid molding and processing frozen samples. Rosanne Stoops conducted the grain-size analysis, Atterberg limits, specific gravity, and organic content tests. Richard Roberts conducted the frost susceptibility tests and some of the compaction tests. Charles Smith determined the remaining compaction curves. Jonathan Ingersoll conducted the hydraulic property tests—moisture retention and hydraulic conductivity. Dr. Patrick Black determined the unfrozen moisture content characteristics. The resilient modulus testing was done by a team of CRREL personnel whose efforts we greatly appreciate. Arthur Peacock, Brian Charest, and David Carbee were all involved in molding, freezing, and milling the specimens. Glenn Durell and Dale Bull conducted the resilient modulus testing. Brian Charest characterized the water content and density subsequent to resilient modulus testing.

CONTENTS

	Page
Preface	ii
Executive summary	vi
Introduction	1
Model description	3
FROST	4
TRANSFORM	4
NELAPAV	5
CUMDAM	6
Material testing	8
Physical characteristics	11
Hydraulic properties	11
Frost susceptibility	13
Unfrozen water content	16
Resilient modulus	17
Performance predictions	26
Phase 1	26
Phase 2A	34
Phase 2B	36
Phase 3	37
Discussion/recommendations	42
Conclusions	44
Literature cited	44
Abstract	46

ILLUSTRATIONS

Figure

1. Location of Mn/ROAD	1
2. Schematic layout of Mn/ROAD	1
3. Mainline asphalt test sections	2
4. Grain size distribution in tested specimens of Mn/ROAD base materials	2
5. Mainline concrete test sections	3
6. Flow chart of mechanistic design procedure	4
7. Comparison of asphalt moduli computed with Schmidt and Ullidtz models	5

Page

8. Stress dependence of resilient modulus in station 1206 clay subgrade material 6
9. Comparison of grain size distribution of substitute materials and specifications for equivalent Mn/ROAD bases 11
10. Grain size distribution in the subgrade materials 12
11. Moisture retention test results 14
12. Tension vs. hydraulic conductivity curves 15
13. Temperature vs. gravimetric unfrozen water content curves 17
14. Frozen and unfrozen modulus data compared with calculated moduli from predictive equations 23
15. Resilient modulus vs. degree of saturation of never-frozen 1206 subgrade material illustrating the effect of dry density 25
16. Resilient modulus vs. degree of saturation illustrating effect of stress parameter 25
17. Distribution of seasonal freezing index with time at Buffalo, Minnesota 26
18. Pavement structure of Mn/ROAD test sections simulated 27
19. Example output from FROST for Mn/ROAD test section ML5-F4 with a 2-m (6-ft) water table 30
20. Seed moduli output by TRANSFORM for Mn/ROAD test section ML5-F4 with a 2-m (6-ft) water table 30
21. Deflection and strain calculated by NELAPAV for Mn/ROAD test section ML5-F4 with a 2-m (6-ft) water table 31
22. Cumulative damage for case f4w6 with “normal” subgrade 33
23. Cumulative damage for case f2w9 33
24. Cumulative damage for case f4w6 with “1232” subgrade 33
25. Cumulative damage for case r5w6 34
26. Frost and thaw penetrations predicted by FROST for freeze seasons in Phase 2B environmental sensitivity study 36
27. Distribution of freezing indices and water table depths in 21-yr Phase 3 series 38
28. Predicted results from simulation of full depth section during freeze season 1983–1984, starting on 1 October 40
29. Predicted results from simulation of full depth section during freeze season 1985–1986, starting on 1 October 40
30. Distribution of accumulative damage during seasons 42

TABLES

Table

1. Results of regression analyses—test soils from Mn/ROAD 6
2. Models currently available in NELAPAV 8
3. Cumulative damage models used 9
4. Laboratory tests performed on Mn/ROAD materials 10

5. Physical properties of Mn/ ROAD materials 12
6. Compaction test results—Mn/ROAD materials 13
7. Coefficients for hydraulic properties in the form of Gardner's equations 13
8. Frost susceptibility test results 16
9. Constants for unfrozen moisture content equations 16
10. Resilient modulus samples tested 19
11. Stress conditions of resilient modulus tests in current study 21
12. Stress conditions of resilient modulus tests—previous study 21
13. Test sections simulated, and maximum frost heave/frost penetration predictions 27
14. Material parameters input to FROST for Mn/ROAD test section simulations 28
15. Predicted applications to failure from Phase 1 simulation series of flexible pavement tests sections 32
16. Applications to failure from simulations of rigid test sections 33
17. Predicted applications to failure from simulations of flexible test sections run in Phase 2A series 35
18. Performance predictions for F3 test section with water table at 2.4 m (8 ft) 37
19. Results of 21-yr freezing index/water table series 38
20. Midfreeze season thaw index summations 41
21. Average percentage of total yearly damage accumulated during four seasons 41

EXECUTIVE SUMMARY

This report describes a study to verify and apply a mechanistic design and evaluation method for pavements in seasonal frost areas that was conducted as a Construction Productivity Advancement Research (CPAR) project between the Minnesota Department of Transportation (Mn/DOT) and the U.S. Army Cold Regions Research and Engineering Laboratory (CRREL). The study involved four components.

1. Mn/DOT constructed a full-scale pavement test facility adjacent to Interstate 94, referred to as the Minnesota Road Research Project (Mn/ROAD). The project includes 23 test cells, which are composed of fourteen asphalt- and nine concrete-surfaced sections. Each cell is 153 m (500 ft) long with transitions of various lengths separating the individual cells. The cells were designed to have a service life of either five or ten years. The test road was opened to traffic in August of 1994.

2. CRREL performed extensive laboratory tests on the base and subgrade materials from the Mn/ROAD test cells to characterize them and their behavior under seasonal frost conditions and to provide input necessary for modeling the materials. Tests included those of physical properties (grain-size distribution, specific gravity, Atterberg limits, organic content, hydraulic properties, and compaction) as well as tests related to freeze/thaw processes (frost susceptibility and unfrozen moisture content) (Bigl and Berg 1996a). Resilient modulus tests with a matrix of applied confining and deviator stresses were also conducted on the Mn/ROAD materials at several temperatures below freezing and at various moisture and density conditions (Berg et al. 1996). All materials exhibited a two to three order of magnitude increase in resilient modulus at subfreezing temperatures of –2°C and lower. When unfrozen, the resilient modulus of all of the materials was stress dependent and also increased as the degree of saturation decreased. For the materials where a variety of densities were tested, modulus was also dependent on density.

3. Laboratory tests provided the input parameters necessary for the third component of the study, modeling with the CRREL Mechanistic Pavement Design and Evaluation Procedure. It consists of four computer programs that compute soil and pavement moisture and temperature conditions (FROST), resilient modulus and Poisson's ratio (TRANSFORM), stresses and strains in the pavement system (NELAPAV), and cumulative damage (CUMDAM). Damage predictions are based on equations that employ horizontal strain at the base of an asphalt layer, vertical strain at the top of the subgrade, or horizontal stress at the base of a concrete layer. The procedure was used to predict pavement performance of some of the Mn/ROAD test sections. The modeling effort was conducted in three phases, which investigated the effects of freeze season characteristics, water table position, asphalt model and subgrade characteristics on the predicted performance of some Mn/ROAD sections (Bigl and Berg 1996b).

The procedure predicted significantly different performance by the different test sections and highly variable results depending on the performance model applied. The simulated performance of the test sections was also greatly affected by the subgrade conditions, e.g., density, soil moisture and water table depth. In general, predictions for the full-depth asphalt sections indicate that they will not fail due to

cracking, but two of the three criteria for subgrade rutting indicate failure prior to the 5- or 10-yr design life of the sections. Conventional sections are predicted not to fail due to subgrade rutting; however, sections including the more frost-susceptible bases in their design are predicted to fail because of asphalt cracking relatively early in their design life. Sections with non-frost-susceptible bases are predicted to fail near the end of their design life.

4. The planned fourth component of the study, using performance data from Mn/ROAD to validate the Mechanistic Pavement Design and Evaluation Procedure, was not accomplished because construction and trafficking of the Mn/ROAD facility were much delayed from the originally intended schedule.

Material Testing and Initial Pavement Design Modeling
Minnesota Road Research Project

SUSAN R. BIGL AND RICHARD L. BERG

INTRODUCTION

Between January 1990 and December 1994, studies to verify and apply a Corps of Engineer-developed mechanistic design and evaluation method for pavements in seasonal frost areas were conducted as a Construction Productivity Advancement Research (CPAR) project between the Minnesota Department of Transportation (Mn/DOT) and the U.S. Army Cold Regions Research and Engineering Laboratory (CRREL). The project involved four components:

1. Laboratory tests on the pavement materials.
2. Predicting performance with the CRREL Mechanistic Pavement Design Procedure.
3. Construction of the Minnesota Road Research Project (Mn/ROAD).
4. Using performance data from Mn/ROAD to validate the Mechanistic Pavement Design and Evaluation Procedure.

Because construction and trafficking of the Mn/ROAD facility was much delayed from the originally planned schedule, the model validation effort was not accomplished.

Mn/ROAD is located on Interstate 94 near Monticello, Minnesota, approximately 40 miles (64.4 km) northwest of the twin cities of Minneapolis/St. Paul. Figure 1 shows the location of Mn/ROAD. Figure 2 illustrates the layout of the test sections. Only the new westbound I-94 test cells were investigated as part of the CPAR project. The mainline section of Mn/ROAD includes a 3-mile (4.8-km), two-lane roadway over which westbound I-94 traffic is diverted. The project includes 23 test cells, which are composed of fourteen asphalt and nine concrete surfaced sections. Each cell is 153 m (500 ft) long with transitions of various lengths separating the individual cells. The cells were designed to have a service life of either five or ten years. A midpoint cross-over will allow traffic to continue using the 10-year cells once the 5-year cells have failed.

Figure 1. Location of Mn/ROAD.

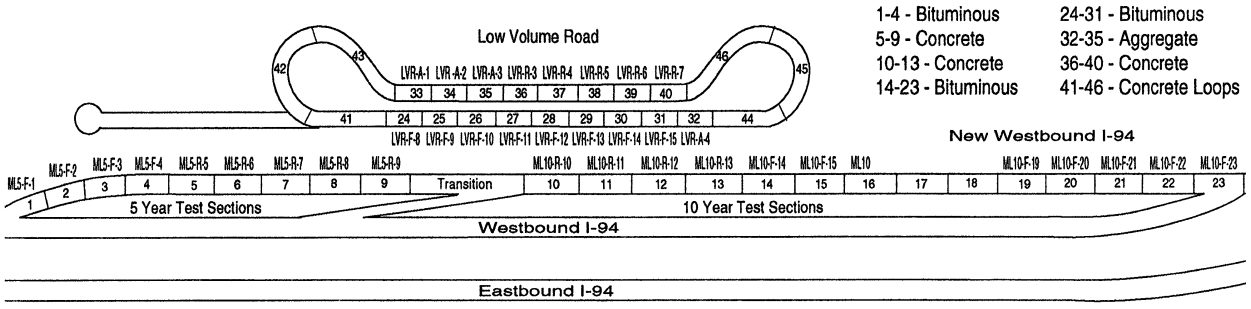

Figure 2. Schematic layout of Mn/ROAD.

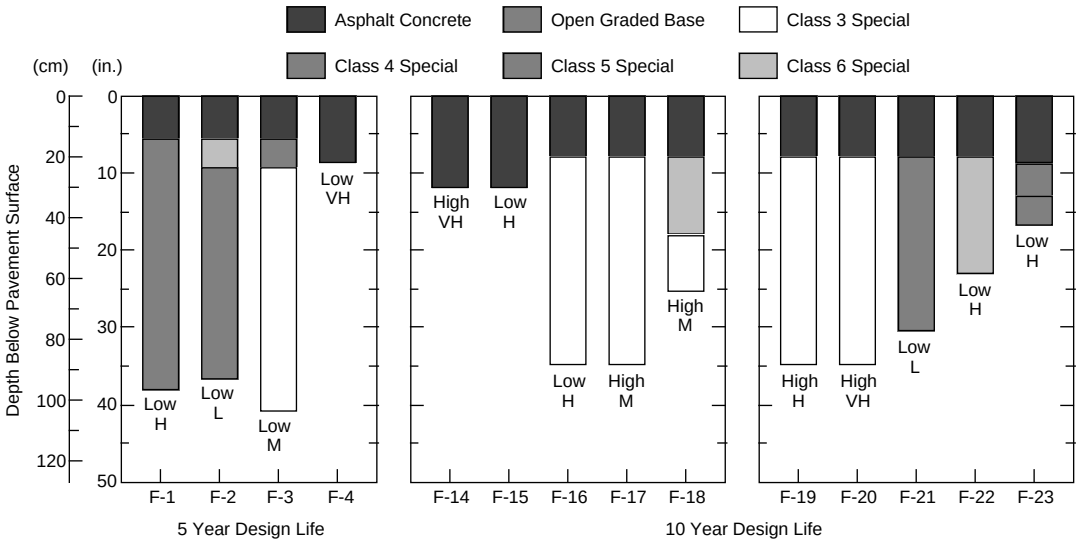

a. 5-yr design life. *b. 10-yr design life.*

Figure 3. Mainline asphalt test sections. In the figure, beneath the base materials, High/Low refer to the asphalt penetration viscosity number; design compactive effort is indicated by VH—very high, H—high, M—medium, and L—low.

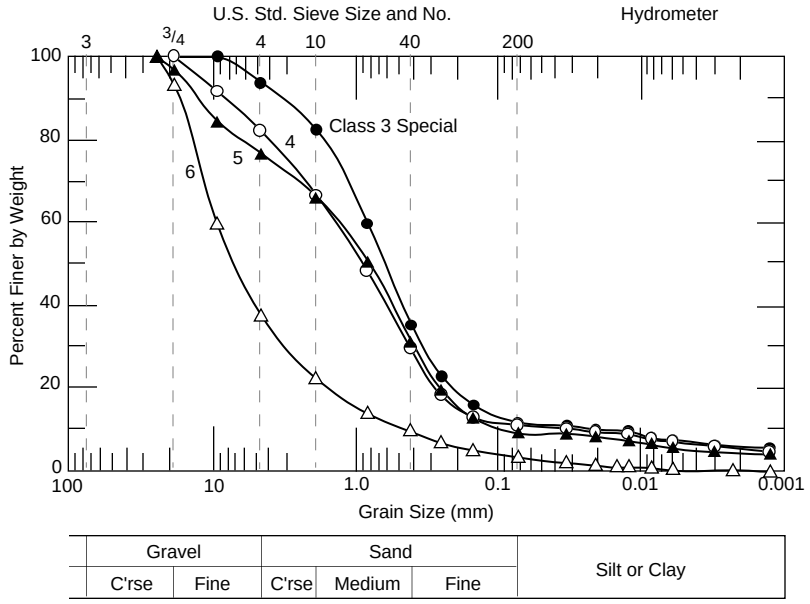

Figure 4. Grain size distribution in tested specimens of Mn/ROAD base materials.

Parameters included in the designs of the asphalt test sections are the thickness and characteristics of the asphalt surface and the presence, thickness and quality of base materials (Fig. 3). The asphalt cement used was an 85/100 pen grade asphalt. The asphalt design included either of two temperature susceptibilities: one with a low penetration viscosity number (PVN) is characteristically more compliant and the other with a high PVN is more brittle. The design compactive effort applied to the asphalt also varies from low to very high, which resulted in varying asphalt cement contents in the field.

The four granular base materials included in the test sections were specified and manufactured to include a range in frost susceptibility (Fig. 4). The class 6 special is a relatively clean, non-frost-susceptible gravel with sand; the special bases,

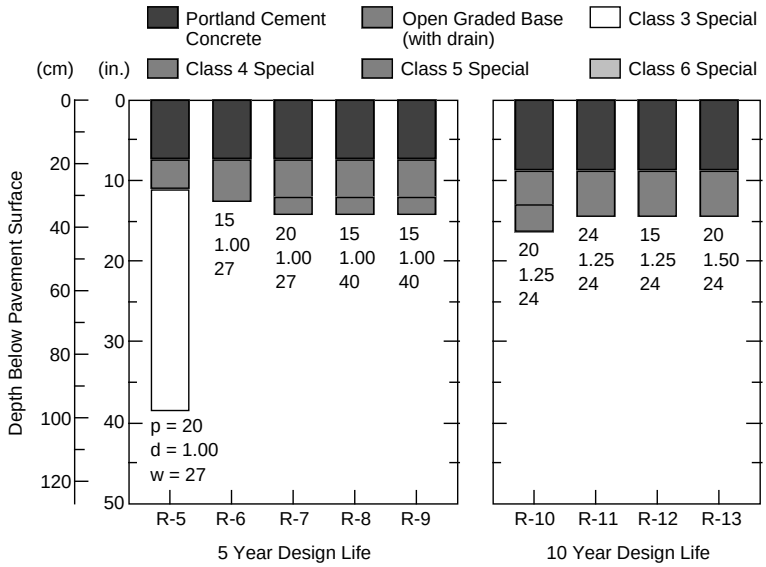

a. 5-yr design life. *b. 10-yr design life.*

Figure 5. Mainline concrete test sections. In the figure, p refers to panel length (ft), d—dowel diameter (in.), w—panel width (ft). Supplemental steel rebar is included in the concrete of 5-year section R-8.

class 5, class 4 and class 3, are all well-graded sands with increasing amounts of finer size particles and associated increasing frost susceptibility. Also included in one of the 10-yr sections is a porous asphalt-stabilized open graded base. The subgrade beneath all test sections is a sandy lean clay. Bigl and Berg (1996a) and Berg et al. (1996) detail properties of the various materials at the site.

In the concrete-surfaced test sections, parameters varied are the thickness of the concrete, panel width and length, dowel diameter, thickness and quality of underlying base materials, and presence of open-graded bases (Fig. 5). The concrete paving surface is plain jointed concrete in all sections, with a constant thickness in the 5-yr and 10-yr sections. Panel lengths vary from 4.6 to 7.3 m (15 to 24 ft); panel widths are 7.3, 8.2, or 12.2 m (24, 27 or 40 ft). Dowel diameters are 2.5, 3.2 or 3.8 cm (1, 1.25, or 1.5 in.). Base materials employed in the concrete sections are similar to those used in the asphalt sections. The subgrade is also a lean clay.

A number of different instrumentation types were installed at Mn/ROAD to measure the environmental conditions at the test sections, the traffic loadings, and the engineering behavior of the materials.

Stage 1 construction took place June 1990 through spring 1992. This effort, which included swamp excavation and backfill, and grading of the test roadway to the top of the base materials, required moving about 765,000 m^3 (1,000,000 yd^3) of material. Completion was significantly delayed due to extremely wet weather during the 1990 and 1991 construction seasons.

Stage 2 construction, which included paving and installation of instrumentation, occurred during the 1992 and 1993 construction seasons. An extensive period of sensor calibration, nondestructive pavement testing and collection of baseline data took place during winter 1993 and spring 1994. The test road was opened to traffic in August of 1994.

Three other reports have been prepared as part of this study (Bigl and Berg 1996a,b and Berg et al. 1996). This report summarizes the results of the other three. If additional details are desired or needed, the other reports should be used.

MODEL DESCRIPTION

A mechanistic pavement design procedure is being developed for use in seasonal frost areas and considers seasonal variations in pavement strength such as:

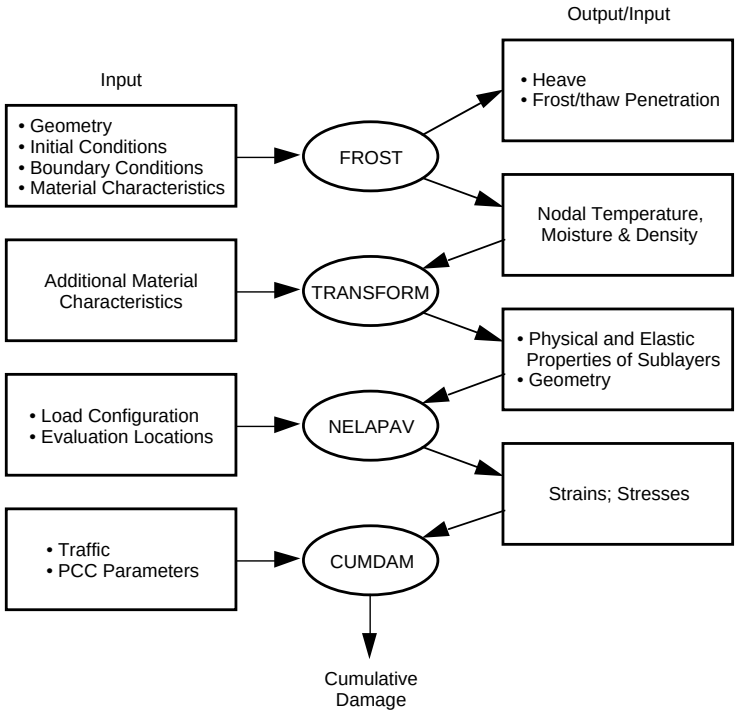

Figure 6. Flow chart of mechanistic design procedure.

1. Large increases in base and subgrade strengths when frozen.
2. Loss of base and subgrade strengths during thawing periods when excess water weakens the layers.
3. Changes in asphaltic concrete strength during the year.

The mechanistic design procedure consists of four computer programs FROST, TRANSFORM, NELAPAV, and CUMDAM (Fig. 6). FROST predicts the amount of frost heave and thaw settlement of the pavement structure and conditions throughout the depth of the structure (temperature, water content, pore water pressure, ice content, density) at a given time increment. TRANSFORM uses the output from FROST as input and divides the pavement structure into "layers" based on moisture or temperature conditions. Each layer is then assigned a resilient modulus, Poisson's ratio and density value. NELAPAV, a nonlinear layered elastic program, calculates stresses, strains and deflections at specified locations within a pavement profile when a load is applied to the surface. CUMDAM calculates the incremental and cumulative damage the pavement undergoes using several available damage models. The behavior is normally modeled for a one-year period, with output on a daily basis. By assuming that the results from a single year will be repeated annually, the number of applications to failure is estimated.

FROST

FROST is a one-dimensional coupled heat flow and moisture flow model that predicts the amount of frost heave and thaw settlement of a pavement or soil profile with time. It also calculates temperatures, pore pressures, water contents, ice contents, and densities through the depth of the profile at each time increment. FROST was originally developed in a cooperative study funded by the Corps of Engineers, the Federal Highway Administration, and the Federal Aviation Administration (Berg et al. 1980). Additional details are given in Guymon et al. (1993) and in Bigl and Berg (1996 b).

TRANSFORM

TRANSFORM was developed at CRREL by Chamberlain et al. (in prep.) and was modified extensively for this study. TRANSFORM uses daily output files from FROST as input and produces layered pavement systems where each layer is assigned a resilient modulus (M_r), Poisson's ratio,

density and thickness. First, a modulus is calculated for each element; then, elements with moduli not differing by more than 20% are combined in a single layer. Output files from TRANSFORM are in the format to be used as input files to NELAPAV. Inputs to and outputs from the TRANSFORM program are discussed in more detail in Bigl and Berg (1996b). The basic equations used to calculate resilient moduli are given here (Table 1).

Moduli of surface paving materials were calculated as follows. PCC (portland cement concrete) had the M_r set at a constant value of 3.4×10^7 kPa (5,000,000 lb/in.^{2}). In the initial two simulation series, the resilient modulus, M_r of asphalt concrete layers were calculated by the Schmidt (1975) equation, which predicted very low summer values. In a third series of simulations, a second model was used for predicting asphalt moduli when the temperature was above 1°C (Ullidtz 1987), and the Schmidt relationship was used when temperatures were below 1°C. Modulus values obtained from the two models are compared in Figure 7.

In layers that represent an unstabilized base course, subbase or subgrade material, TRANSFORM calculates the modulus using regression equations developed from results of laboratory resilient modulus testing conducted on frozen and thawed soil samples. The equations relate the frozen resilient modulus to temperature (through unfrozen water content), and the unfrozen resilient modulus to degree of saturation, stress condition, and (when available) to density (Table 1).

NELAPAV

The program NELAPAV, an acronym for **n**onlinear **e**lastic **l**ayer **a**nalysis for **pav**ements, computes stresses, strains, and displacements at any point in an n-layered pavement system. The mainframe computer version of the program was developed for CRREL by Lynne Irwin of Cornell University and Gregor Fellers of CRREL in 1980. Further refinements such as a microcomputer version were developed by Lynne Irwin and Daniel Speck at Cornell University in 1984 and 1985 (Irwin and Speck 1986). The program uses the Chevron Layered Elastic Systems program (CHEVLAY) to calculate the elastic stresses and strains in a multiple layer system.

The primary reason NELAPAV was chosen is because it allows the use of nonlinear (i.e., stress-dependent) modulus values in the analysis. Modulus values for thawing and unfrozen fine-grained soils are highly nonlinear as illustrated in Figure 8. Table 2, from Yang (1988), illustrates the various types of linear and nonlinear models currently available for use in NELAPAV; however, models 2 and 7 are not currently incorporated in the rest of the design procedure.

Daily output from NELAPAV includes 1) a repeat of the input information, 2) moduli of the

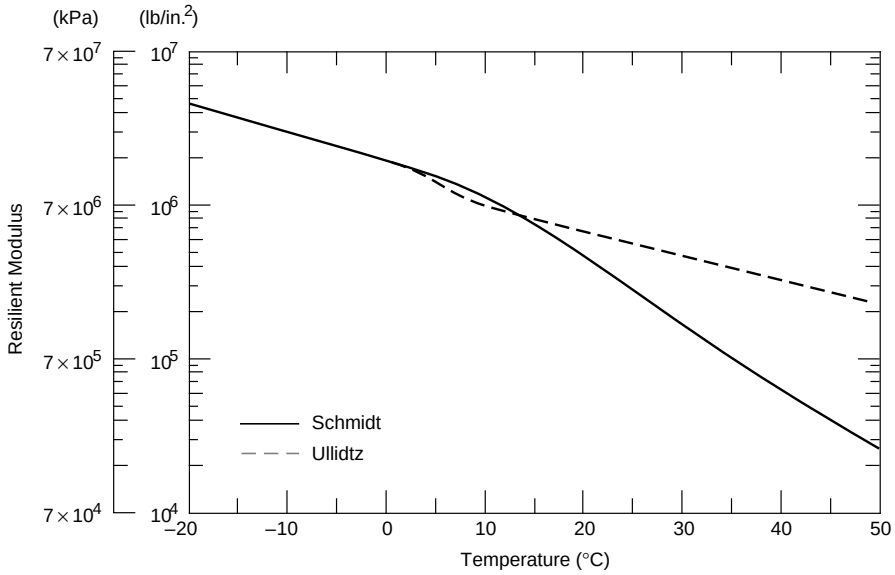

Figure 7. Comparison of asphalt moduli computed with Schmidt and Ullidtz models.

Table 1. Results of regression analyses—test soils from Mn/ROAD.

A. Frozen condition.

Material	*Equation (M_r in lb/in.^{2})**	n	r^2	*Std error*
Clay subgrade sample 1206 (565)				
Frozen	$M_r = 1,087\, f(w_u)^{-5.259}$	207	0.99	0.319
Frozen	$M_r = 1,049\, f(w_{u-g})^{-2.344}$	207	0.99	0.275
Frozen	$M_r = 1,052\, f(w_{u-v})^{-2.929}$	207	0.99	0.262
Clay subgrade sample 1232 (566)				
Frozen	$M_r = 905\, f(w_u)^{-4.821}$	244	0.98	0.378
Frozen	$M_r = 846\, f(w_{u-g})^{-2.16}$	244	0.98	0.423
Frozen	$M_r = 848\, f(w_{u-v})^{-2.633}$	244	0.98	0.394
Class 3 "stockpile"				
Frozen	$M_r = 5,824\, f(w_u)^{-2.026}$	186	0.97	0.491
Frozen	$M_r = 5,488\, f(w_{u-g})^{-1.076}$	210	0.97	0.507
Frozen	$M_r = 5,542\, f(w_{u-v})^{-1.249}$	186	0.97	0.467
Class 4 (taxiway A subbase)				
Frozen	$M_r = 2,826\, f(w_u)^{-5.220}$	69	0.92	0.835
Frozen	$M_r = 1,813\, f(w_{u-g})^{-1.733}$	85	0.93	0.885
Frozen	$M_r = 1,652\, f(w_{u-v})^{-2.813}$	69	0.91	0.916
Class 5 (dense graded stone)				
Frozen	$M_r = 11,320\, f(w_u)^{-2.036}$	28	0.97	0.404
Frozen	$M_r = 8,695\, f(w_{u-g})^{-1.2814}$	28	0.95	0.511
Frozen	$M_r = 9,245\, f(w_{u-v})^{-1.489}$	28	0.97	0.432
Class 6 "stockpile"				
Frozen	$M_r = 19,924\, f(w_u)^{-1.243}$	260	0.98	0.372
Frozen	$M_r = 19,427\, f(w_{u-g})^{-0.795}$	260	0.98	0.338
Frozen	$M_r = 19,505\, f(w_{u-v})^{-0.897}$	260	0.98	0.341

layers resulting from calculations, and 3) stress conditions for all points specified. For this study, the points specified were located 0.01 in. above the bottom of the asphalt or PCC and 0.01 in. below the top of the subgrade. In the program, a 4090-kg (9,000-lb) load was applied to a 15-cm (5.91-in.) radius, which approximates the area of a standard set of dual wheels or a falling weight deflectometer (FWD) testing plate.

CUMDAM

The program CUMDAM calculates cumulative damage to the pavement structure, and was developed at CRREL. In general form, the procedure used for CUMDAM's calculations is the linear

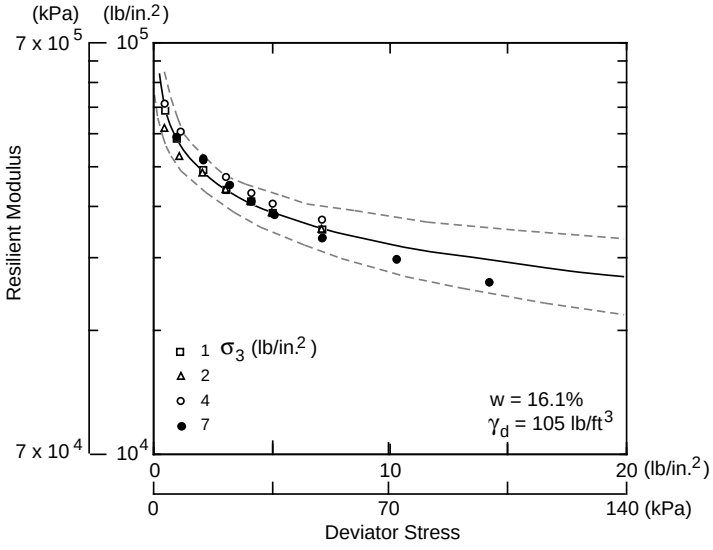

Figure 8. Stress dependence of resilient modulus in station 1206 clay subgrade material (from Bigl and Berg 1996a).

Table 1 (cont'd).

B. Unfrozen condtion.

Material	*Equation (M_r in lb/in.^{2})*	n	r^2	*Std error*
Clay subgrade sample 1206 (565)				
Never frozen	$M_r = 1,597,000\, f(S)^{-2.63}\, f(\gamma)^{14.42}\, f_3(\sigma)^{-0.257}$	655	0.82	0.251
Clay subgrade sample 1232 (566)				
Never frozen	$M_r = 1.518 \times 10^{30}\, f(S)^{-13.85}\, f_3(\sigma)^{-0.272}$	451	0.95	0.328
Class 3 "stockpile"				
Thawed	$M_r = 283,300\, f(S)^{-1.003}\, f_2(\sigma)^{0.206}$	408	0.86	0.520
Class 4 (taxiway A subbase)				
Thawed	$M_r = 8.946 \times 10^{8}\, f(S)^{-3.026}\, f_2(\sigma)^{0.292}$	149	0.86	0.168
Class 5 (dense graded stone)				
Thawed	$M_r = 382,400\, f(S)^{-0.8759}\, f_2(\sigma)^{0.1640}$	64	0.77	0.164
Class 6 "stockpile"				
Thawed	$M_r = 1,391\, f(S)^{-0.507}\, f(\gamma)^{4.04}\, f_1(\sigma)^{0.608}$	492	0.79	0.232
Thawed	$M_r = 5,257\, f(S)^{-0.486}\, f(\gamma)^{4.05} e^{0.0193 f_1(\sigma)}$	492	0.76	0.249

Notes:

n = number of test points
r^2 = coefficient of determination
M_r = resilient modulus
$f(S)$ = S/S_o
S = degree of saturation (%)
S_o = 1.0 %
$f(\gamma)$ = γ_d/γ_0
γ_d = dry density (Mg/m^3)
γ_0 = 1.0 Mg/m^3
$f(w_u)$ = w_{u-g}/w_t
w_{u-g} = gravimetric unfrozen water content
w_t = gravimetric total water content
$f(w_{u-g})$ = w_{u-g}/w_o
w_o = unit water content (1.0)
$f(w_{u-v})$ = w_{u-v}/w_o
w_{u-v} = volumetric unfrozen water content
σ = stress (lb/in.^{2})
$f_1(\sigma)$ = J_1/σ_o
$f_2(\sigma)$ = $(J_2/t_{oct})/\sigma_o$
$f_3(\sigma)$ = τ_{oct}/σ_o
σ_o = 1.0 lb/in.^{2}
J_1 = bulk stress (lb/in.^{2})
J_1 = $3\sigma_3 + \sigma_d$
J_2 = 2nd stress invariant (lb/in.^{2})
J_2 = $3\sigma_3^2 + 2\sigma_3\sigma_d$
τ_{oct} = octahedral shear stress (lb/in.^{2})
τ_{oct} = $\left(\sqrt{2}/3\right)\sigma_d$

*Output from equations can be converted to kPa by multiplying by 6.895.

summation of cycle ratios, referred to as Miner's rule, which may be stated as:

$$\sum_{i=1}^{i} \frac{n_i}{N_i} = D \qquad (1)$$

where n_i = number of applications at strain level i
N_i = number of applications to cause failure at strain level i, based on damage model predictions
D = total cumulative damage.

In this relation, failure occurs when D equals or exceeds 1.0. Thus, for a section to last its design life, the value of D cannot accumulate to 1.0 until the design period expires.

The value n_i relates to the design traffic, or applications, in 8165-kg (18,000-lb) equivalent standard axle loadings (ESALs). For the two initial modeling series of this study, traffic was anticipated to be 2,815,000 ESALs during a 5-yr period. Loadings were applied on a daily basis at a constant rate of 1542 ESALs per day. In the

Table 2. Models currently available in NELAPAV (from Yang 1988).

Model no.	*Name*	*Specification*
0	Linear	M_r = constant
1	Bulk stress	$M_r = k_1\theta^{k_2}$
2	Deviator stress	$M_r = \begin{cases} k_2 + k_3(k_1 - \sigma_d) & \sigma_d < k_1 \\ k_2 + k_4(\sigma_d - k_1) & \sigma_d \geq k_1 \end{cases}$
3	Second stress invariant	$M_r = k_1(J_2/\tau_{oct})^{k_2}$
4	Octahedral shear stress	$M_r = k_1{\tau_{oct}}^{k_2}$
5	Vertical stress	$M_r = k_1{\sigma_v}^{k_2}$
6	Major principal stress	$M_r = k_1{\sigma_1}^{k_2}$
7	First stress invariant octahedral shear stress and anisotropic consolidation ratio	$M_r = k_1(J_{10}^2 + J_{1p}^2)^{k_2}(1+\tau_{oct})^{k_3}{k_c}^{k_4}$

Notes:

θ = bulk stress
k_1, k_2, k_3, k_4 = constants
σ_d = deviator stress
σ_v = vertical stress
σ_1 = major principal stress
J_{10} = first stress invariant due to overburden only
J_{1p} = first stress invariant due to overburden and load
k_c = anisotropic consolidation ratio

third simulation series, the anticipated traffic was revised to 3,300,000 ESALs during 5 years, applied at a rate of 1808 ESALs per day.

CUMDAM includes several damage models previously developed for determining N_i (Table 3). Of the damage models for flexible pavements, four are based on horizontal strain at the bottom of the asphalt layer, and relate to damage effects that result in fatigue pavement cracking. These models were developed by the Asphalt Institute (1982), Witczak (1972), the Corps of Engineers (U.S. Army 1988), and Coetzee and Connor (1990). Three other damage models for flexible pavements are based on the vertical strain at the top of the subgrade, and these relate to subgrade rutting damage in the pavement. They were developed by the Asphalt Institute (1982), the Federal Aviation Administration (Bush 1980), and the Corps of Engineers (U.S. Army 1987). For rigid pavements, CUMDAM uses the damage model developed by the Corps of Engineers (U.S. Army 1990), which is based on the horizontal stress at the base of the PCC.

The program assumes that all applications will pass over the location being modeled. That is, the damage is not reduced according to a pass-to-coverage algorithm to simulate the lateral wander of the axle within the travel lane. It is recognized that some of the equations are being applied outside the original assumptions used in their development; however, they are representative of cumulative damage models currently available and are used for the initial analysis until more appropriate equations can be determined.

MATERIAL TESTING

CRREL conducted various laboratory tests on base and subgrade materials from Mn/ROAD, with

Table 3. Cumulative damage models used.

A. Flexible pavement horizontal strain criteria

1) The Asphalt Institute (MS-1, 1982):

$$N_a = 18.4\ C\ (4.325\times10^{-3})\left|\varepsilon_t\right|^{-3.291}\left[E_a{}^{-0.854}\right]$$

where N_a = number of load applications to 45% cracking
C = a function of the volume of the voids and the volume of asphalt, 10^z
z = $4.84\ [(V_b/V_v + V_b) - 0.69]$
V_b = volume of the asphalt, percent (11%)
V_v = volume of the voids, percent (5%)
ε_t = tensile strain at the bottom of the asphalt layer, in./in.
E_a = modulus of the asphalt layer, lb/in.^{2}

2) Witczak (1972) (also Asphalt Institute MS-11):

$$N_a = ab^{q^d}\,(1/\varepsilon_t)^c$$

where a = 1.86351×10^{-17}
b = 1.01996
c = 4.995
d = 1.45
q = pavement temperature, °F

3) The Corps of Engineers (U.S. Army 1988):

$$N_a = 10^{(2.68-5\log\left|\varepsilon_t\right|-2.66\log E_a)}$$

4) Coetzee and Connor (1990):

$$N_a = a\ \varepsilon_t{}^b E_a{}^c$$

where, when $E_a \geq$ 1,500,000 lb/in.^{2}: a, b, c
$= 3.364\times10^6, -7.370, -4.470$
and when $E_a <$ 1,500,000 lb/in.^{2}: a, b, c
$= 6.565\times10^6, -5.764, -3.640$

B. Flexible pavement subgrade strain criteria

1) The Asphalt Institute (1982):

$$N_s = 10^{[1/m\ (\log l - \log\varepsilon_v)]}$$

where N_s = allowable traffic based on subgrade strain
m = a constant (0.25)
l = a constant (2.8×10^{-2})
ε_v = vertical strain at the top of the subgrade, in./in.

2) The Corps of Engineers (U.S. Army 1987):

$$N_s = 10000\,(A/\varepsilon_v)^B$$

where A = 0.000247 + 0.00245 log E_s
B = $0.0658\ E_s{}^{0.559}$
E_s = subgrade resilient modulus, lb/in.^{2}

C. Rigid pavement horizontal stress criteria

1) The Corps of Engineers (U.S. Army 1990):

$$N_h = 10^{\,[(df - adon)/bdon]}$$

where: N_h = allowable traffic based on horizontal stress
df = R_{con}/σ_h
R_{con} = flexural strength of the concrete, lb/in.^{2}
σ_h = horizontal stress at the base of the concrete, lb/in.^{2}
$adon$ = 0.2967 + 0.002267 SCI
$bdon$ = 0.3881 + 0.000039 SCI
SCI = surface condition index of the pavement when failed

emphasis on tests to provide input to the Mechanistic Pavement Design Procedure (Table 4). Tests to generally characterize physical properties included grain-size distribution, specific gravity, Atterberg limits, organic content, hydraulic properties (moisture retention and hydraulic conductivity), and compaction. Tests more specifically related to freeze/thaw processes were frost susceptibility and unfrozen moisture content at subfreezing temperatures. Resilient modulus values were also determined in both the frozen and thawed (or unfrozen) condition. Modeling materials with the CRREL design procedure requires data from the following tests: moisture retention, hydraulic conductivity, unfrozen moisture content, and resilient modulus.

This report provides a brief summary of the testing results; a complete presentation is found in Bigl and Berg (1996a, b) and Berg et al. (1996). The Mn/ROAD test sections include four base

Table 4. Laboratory tests performed on Mn/ROAD materials.

	Physical properties								
Material	*Grain size*	*Specific gravity*	*Atterberg limits*	*Organic content*	*Hydraul prop.*	*Compact test*	*Frost suscept.*	*Unfrozen moisture*	*Resilient modulus*
Subgrade									
1171*	o	o	o	o	o	o	o	o	–
1193*	o	o	o	o	–	o	o	o	–
1206	o	o	o	o	o	o	o	o	o
1232	o	o	o	o	o	o	o	o	o
Class 3 sp									
stockpile	o	o	o	–	o	o	o	o	o
Class 4 sp									
TAS†	•	•	–	–	•	–	–	–	•
test strip	F	o	–	–	P	–	o	o	F
Class 5 sp									
DGS**	•	•	•	–	•	–	•	–	•
stockpile	F	o	–	–	F	–	F	o	P
Class 6 sp									
stockpile	o	o	–	–	o	o	o	o	o

Notes:
o work completed in this study
• data from other studies
P presently being conducted
F planned future work
– no plan to complete this cell in test matrix
"test strip" materials were taken from inplace test strip adjacent to Mn/ROAD
"stockpile" materials were furnished from stockpiles manufactured for the Mn/ROAD project
* Test results from this subgrade sample are in separate reports—see text.
† TAS, taxiway A subbase (substitute material for modeling)
** DGS, dense graded stone (substitute material for modeling)

materials that were specified to include a range of frost susceptibility. Of the four bases, the two extreme gradations (class 3 special and class 6 special) were tested for all properties. Testing of the two intermediate base materials (class 4 special and class 5 special) was accomplished after this study was complete. Two subgrade samples received the full series of tests. They are referred to with the project station number where they had been collected—1206 and 1232*. Tests were also conducted to determine general physical characteristics, unfrozen moisture, and frost susceptibility of two subgrade samples from stations 1171 and 1193. Since their properties were similar to the 1232 and 1206 samples, respectively, they were not tested for resilient modulus.

Because materials for the two intermediate bases were unavailable when the initial laboratory testing for the pre-1993 modeling portions of this study were conducted, their behavior was approximated using data from previously tested materials that most closely matched their specified size gradations. A subbase from taxiway A at the Albany, New York, airport most closely matched the class 4 special subbase specifications; dense-graded stone from Winchendon, Massachusetts, most closely matched the class 5 special material (Fig. 9). These materials are referred to here, respectively, as TAS and DGS.

*The original Mn/DOT sample numbers for the subgrade samples were 563 for 1171, 564 for 1193, 565 for 1206, and 566 for 1232.

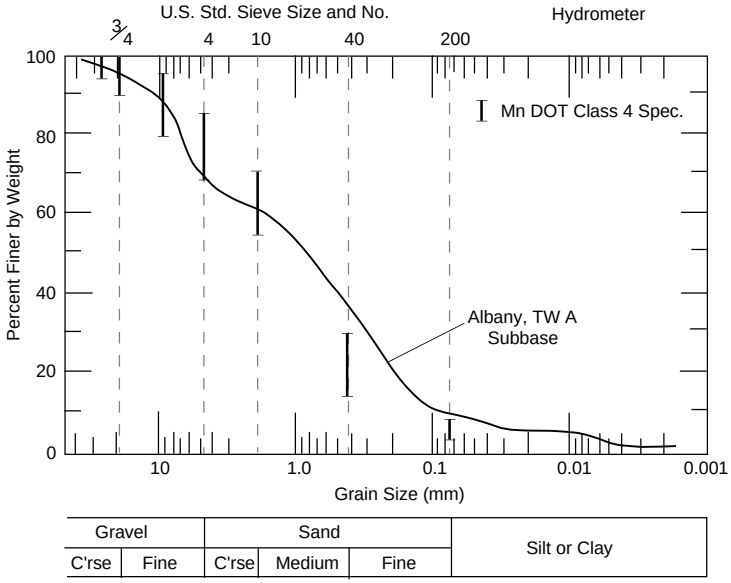

a.Taxiway A subbase, Albany, New York/ class 4 special base.

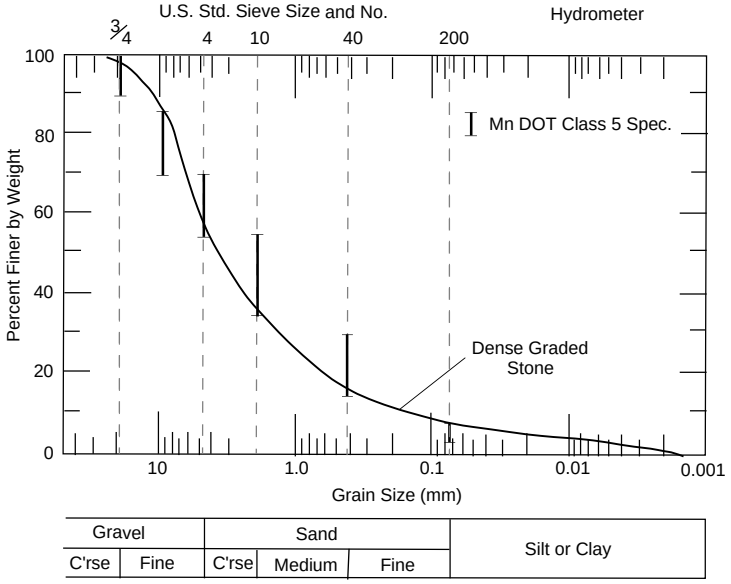

b. Dense-graded stone, Winchendon, Massachusetts/class 5 special base.

Figure 9. Comparison of grain size distribution of substitute materials and specifications for equivalent Mn/ROAD bases.

Physical characteristics

The general physical properties of the Mn/ ROAD materials were tested according to standard techniques (Table 5). Grain size gradations of the base materials were shown in Figure 4; gradations of the subgrades classified them as sandy lean clays (Fig. 10). Maximum density and optimum moisture content determined in compaction testing are listed in Table 6.

Hydraulic properties

The moisture retention and hydraulic conductivity tests were conducted using the procedures outlined in Ingersoll (1981). A typical test begins with a saturated sample that is dried incrementally to determine point values of moisture content and pore pressure head. The laboratory data are fitted with an equation in the form of Gardner's (1958) function using a least squares

Table 5. Physical properties of Mn/ROAD materials.

Material	*Classification**	*Specific gravity*†	*Atterberg limits*** *LL*	*PI*	*Organic content*†† *(%)*
Subgrade					
1206	CL, Sandy lean clay	2.70	37.0	18.5	1.5
1232	CL, Sandy lean clay	2.71	26.4	10.9	0.7
Class 3					
stockpile	SW, Well-graded sand	2.69	17.0***	1.2***	—
Class 4					
TAS†††	SM, Silty sand	2.73	—	—	—
Class 5					
DGS†††	GW, Well-graded gravel with sand	2.81	23***	3***	—
Class 6					
stockpile	GW, Well-graded gravel	2.74	—	—	—

* Classification: ASTM D422-63/ASTM D2487-83
† Specific gravity: ASTM D854-83
**Atterberg limits: ASTM D4318-84
†† Organic content: ASTM D2974-87, Method C; maximum furnace temperature 500°C
*** Minus no. 40 sieve fraction.
††† Substitute materials for modeling: TAS: taxiway A subbase; DGS: dense graded stone.

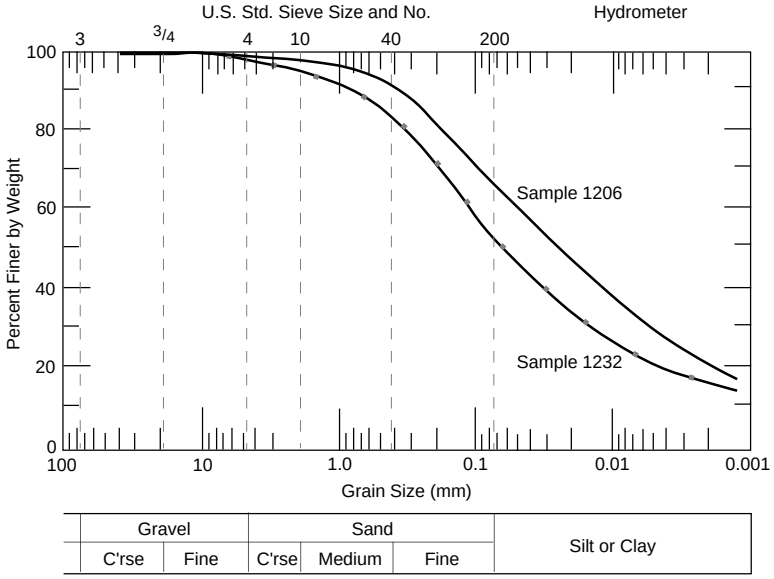

Figure 10. Grain size distribution in the subgrade materials.

approach to determine the best fit parameters A_w and α (Table 7). The equation employed is as follows:

$$\theta_u = \frac{\theta_0}{A_w \left| h_p \right|^{\alpha} + 1} \qquad (2)$$

where θ_u = volumetric water content (%)
θ_0 = soil porosity (%)
h_p = pore pressure head (cm of water)
A_w = Gardner's multiplier for the moisture characteristics
α = Gardner's exponent for the moisture characteristics.

Table 6. Compaction test results—Mn/ROAD materials.

Material	*Maximum dry density Mg/m³ (lb/ft³)*	*Optimum water content (wt %)*	*Method employed*
Subgrade			
1206	1.89 (117.8)	15.5	CE-55
1206	1.69 (105.5)	18.0	CE-12
1206	1.64 (102.1)	20.4	CE-5
1232	1.99 (124.4)	11.9	CE-55
Class 3 special			
stockpile	2.11 (131.8)	7.6	CE-55
stockpile	1.98 (123.7)	11.0	CE-12
Class 4 special			
stockpile	2.01 (126.0)	10.0	T-99*
Class 5 special			
stockpile	2.12 (132.7)	8.1	T-99*
Class 6 special			
stockpile	2.09 (130.4)	2.1	CE-55
stockpile	1.93 (120.8)	4.0	CE-12

Notes:
Tests conducted according to Army methods (MIL-STD-621A):
CE-55 (similar to AASHTO T-180/Modified Proctor); compactive effort: 2,630 kJ/m^3 (55,000 ft-lb/ ft^3)
CE-12 (similar to AASHTO T-99/Standard Proctor); compactive effort: 575 kJ/m^3 (12,000 ft-lb/ft^3)
CE-5—compactive effort: 239 kJ/m^3 (5,000 ft-lb/ft^3)
*Results of Mn/DOT testing

In a similar manner, point values of hydraulic conductivity determined at various pore pressure conditions were fit with a Gardner's form equation using a least squares approach to determine the best fit parameters A_K and β (Table 7).

$$K_H = \frac{k_s}{A_K \left| h_p \right|^{\beta} + 1} \quad (3)$$

where K_H = unsaturated hydraulic conductivity (cm/hr)
k_s = saturated hydraulic conductivity (cm/hr)
A_K = Gardner's multiplier for hydraulic conductivity
β = Gardner's exponent for hydraulic conductivity.

Typical moisture retention and hydraulic conductivity test results are shown in Figures 11 and 12.

Frost susceptibility

Frost susceptibility tests were conducted using the procedures described in Chamberlain (1987). Frost susceptibility is determined by subjecting a soil sample to two freezing cycles and determining the heave rate during the first

Table 7. Coefficients for hydraulic properties in the form of Gardner's equations.

	Moisture retention		*Hydraulic conductivity*	
Material	A_w	α	A_K	β
Subgrade				
1206	0.002399	0.7134	0.0005713	2.6395
1232	0.002260	0.6790	0.001885	1.8129
Class 3 special				
stockpile*	0.1735	0.3239	1647.1	0.7207
Class 4 special				
TAS†	0.1520	0.2690	6.59×10^{-5}	2.9620
Class 5 special				
DGS	0.4961	0.3660	3.912	1.3930
Class 6 special				
blended**	1.0001	0.4444	1.0729×10^{-6}	5.8979

* "Stockpile" materials were furnished from stockpiles manufactured for Mn/ROAD
† Substitute materials for modeling: TAS: taxiway A subbase; DGS: dense graded stone
** "Blended" materials were created by mixing separate size fractions

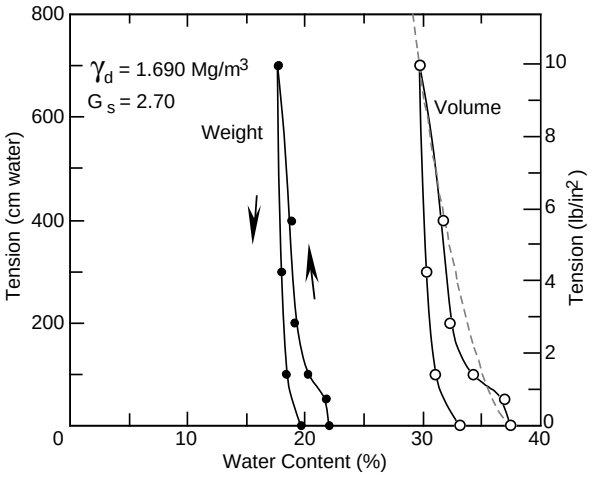

a. Subgrade sample 1206.

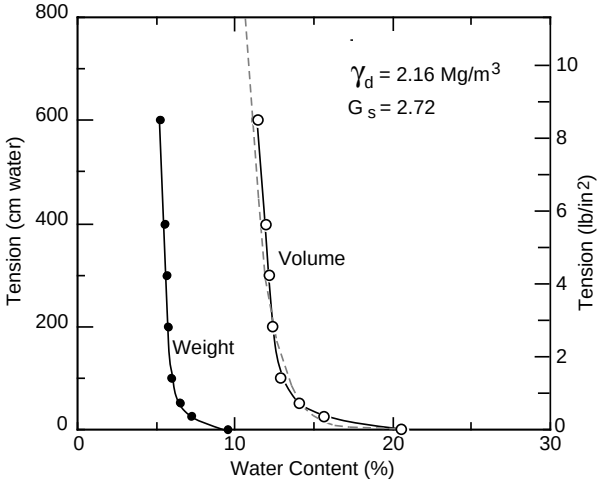

d. Taxiway A subbase.

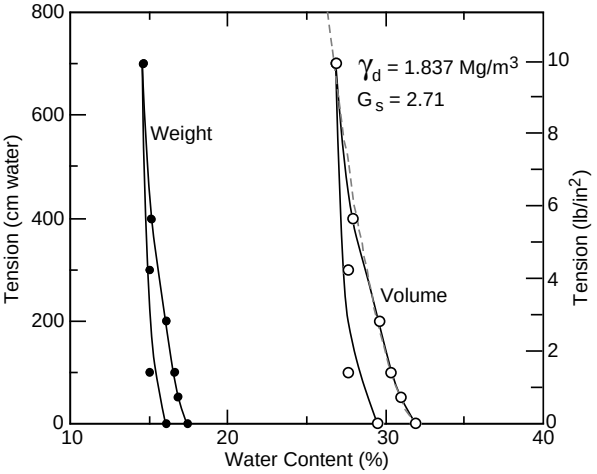

b. Subgrade sample 1232.

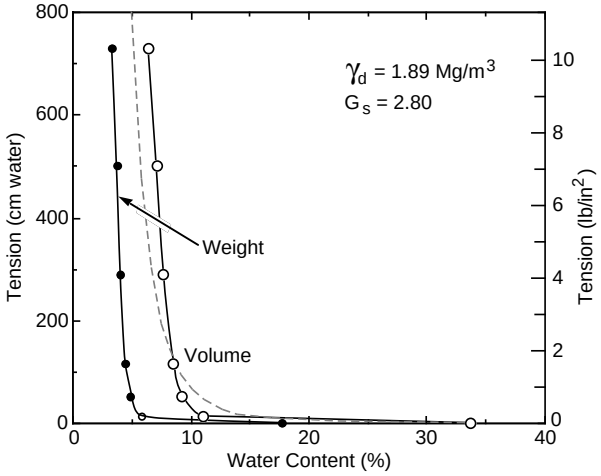

e. Dense-graded stone.

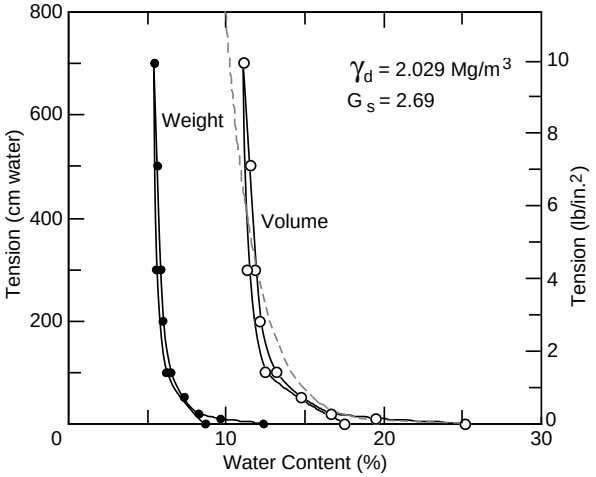

c. Class 3 stockpile.

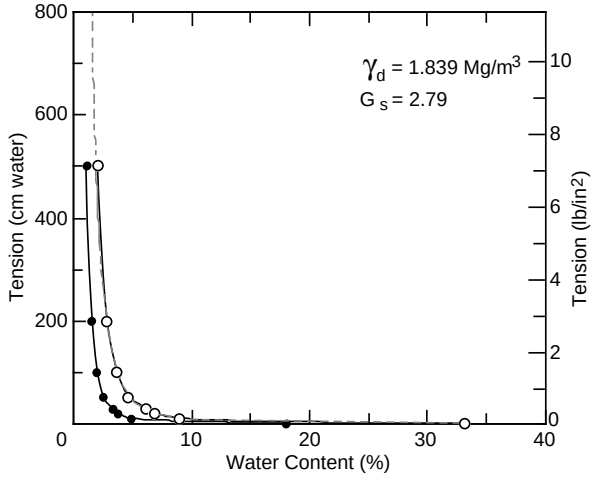

f. Class 6 blended.

Figure 11. Moisture retention test results. Dashed line represents Gardner's equation approximation of the extraction data.

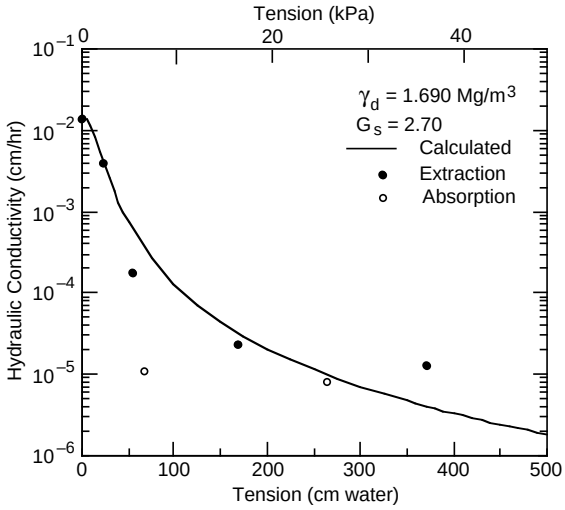

a. Subgrade sample 1206.

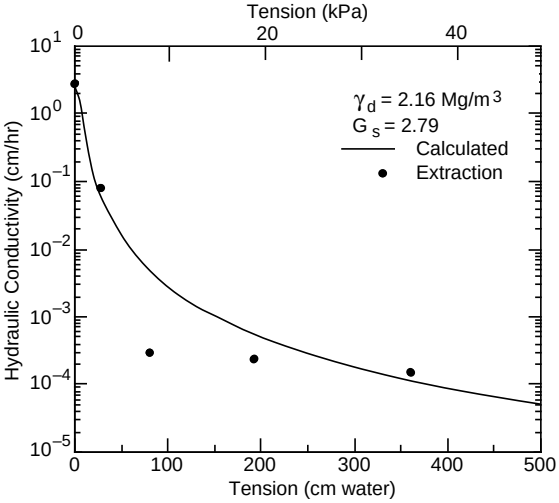

d. Taxiway A subbase.

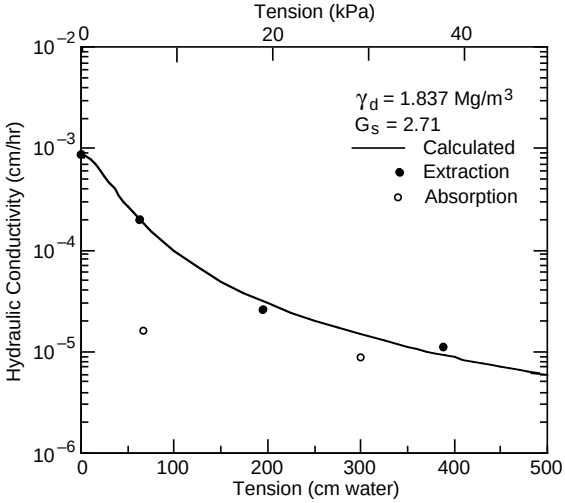

b. Subgrade sample 1232.

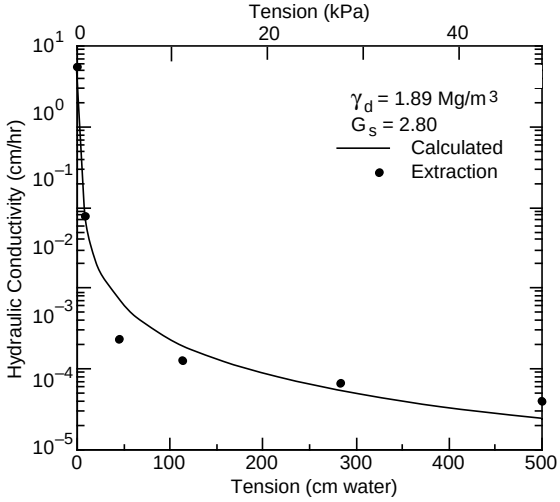

e. Dense-graded stone.

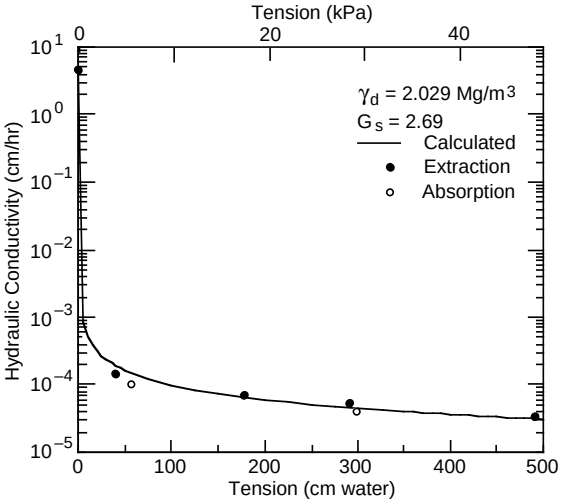

c. Class 3 stockpile.

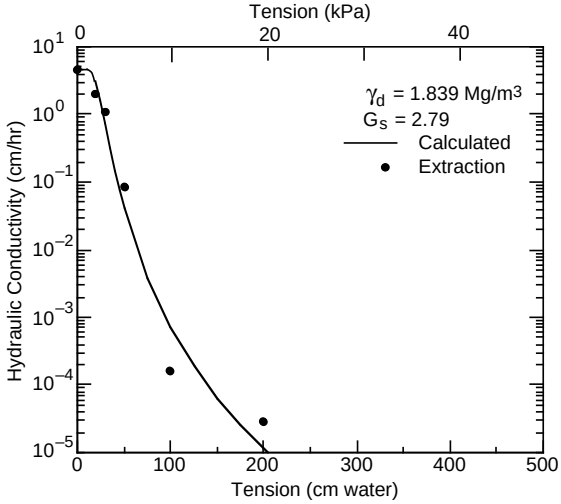

f. Class 6 blended.

Figure 12. Tension vs. hydraulic conductivity curves. Solid line represents Gardner's equation approximation of the extraction data.

Table 8. Frost susceptibility test results.

	1st Freeze cycle		*2nd Freeze cycle*		*CBR test*		
Material	*Hv rate (mm/day)*	*Rating*	*Hv rate (mm/day)*	*Rating*	*CBR (%)*	*Rating††*	*Overall rating*
Subgrade							
1206	9.3	High	16	High	<1	V. high	V. high
1232	1	V. low	7.5	Medium	2	High	High
Class 3 special							
stockpile*	10.5	High	14.5	High	5.5	Medium	High
Class 4 special							
TAS†	10.7	High	12.4	High	3.5	High	High
Class 5 special							
DGS†	3.7	Low	4.5	Medium	10	Low	Medium
Class 6 special							
blended**	<1	Negl.	<1	Negl.	29	Negl.	Negl.

* "Stockpile" materials were furnished from stockpiles manufactured for Mn/ROAD

† Substitute material for modeling: TAS: taxiway A subbase; DGS: dense graded stone

** "Blended" materials were created by mixing separate size fractions

†† Frost susceptibility rating

8 hours of each cycle. The 8-hr heave rate is then converted to an equivalent heave rate in millimeters/day. The heave rate from the two cycles can vary significantly, especially if the soil contains large amounts of clay. At the completion of the test, a CBR test is run on the thawed sample to determine an index of the thaw weakening of the soil. The sample's frost susceptibility classification is then determined using the criteria shown in Chamberlain (1987). Results from these tests are used as a relative index rather than a quantitative predictor of behavior.

Table 8 summarizes the frost susceptibility test results on the Mn/ROAD materials. The heave rate value listed for the base materials is an average determined from multiple samples. Of the two clay subgrades, the 1206 sample had an overall frost susceptibility ranked as very high; the 1232 subgrade ranked as high. The base materials had test results with a range in frost susceptibility. Class 6 special ranked as negligible and class 3 special ranked as high in frost susceptibility. Dense graded stone, used as a substitute for the class 5 special ranked as medium, and Albany taxiway A subbase, the substitute for the class 4 special, ranked high in frost susceptibility.

Unfrozen water content

The variation of unfrozen moisture content with temperature was determined using a pulsed nuclear magnetic resonance (NMR) technique (Tice et al. 1982). The cooling curve data are presented in Figure 13. The figure also include curves of calculated values used to represent the data in

Table 9. Constants for unfrozen moisture content equations (expressed as a percentage).

Material	α	β
Subgrade		
1206	11.085	–0.274
1232	8.121	–0.303
Class 3		
stockpile*	1.497	–0.709
Class 4		
TAS †	3.0**	–0.25**
Class 5		
DGS †	2.0**	–0.4**
Class 6		
stockpile		
+ No. 30	0.232	–1.461
– No. 30	0.567	–1.115

* "Stockpile" materials were furnished from stockpiles manufactured for Mn/ROAD

† Substitute material for modeling: TAS: Taxiway A subbase; DGS: Dense graded stone

**Estimated; no data available

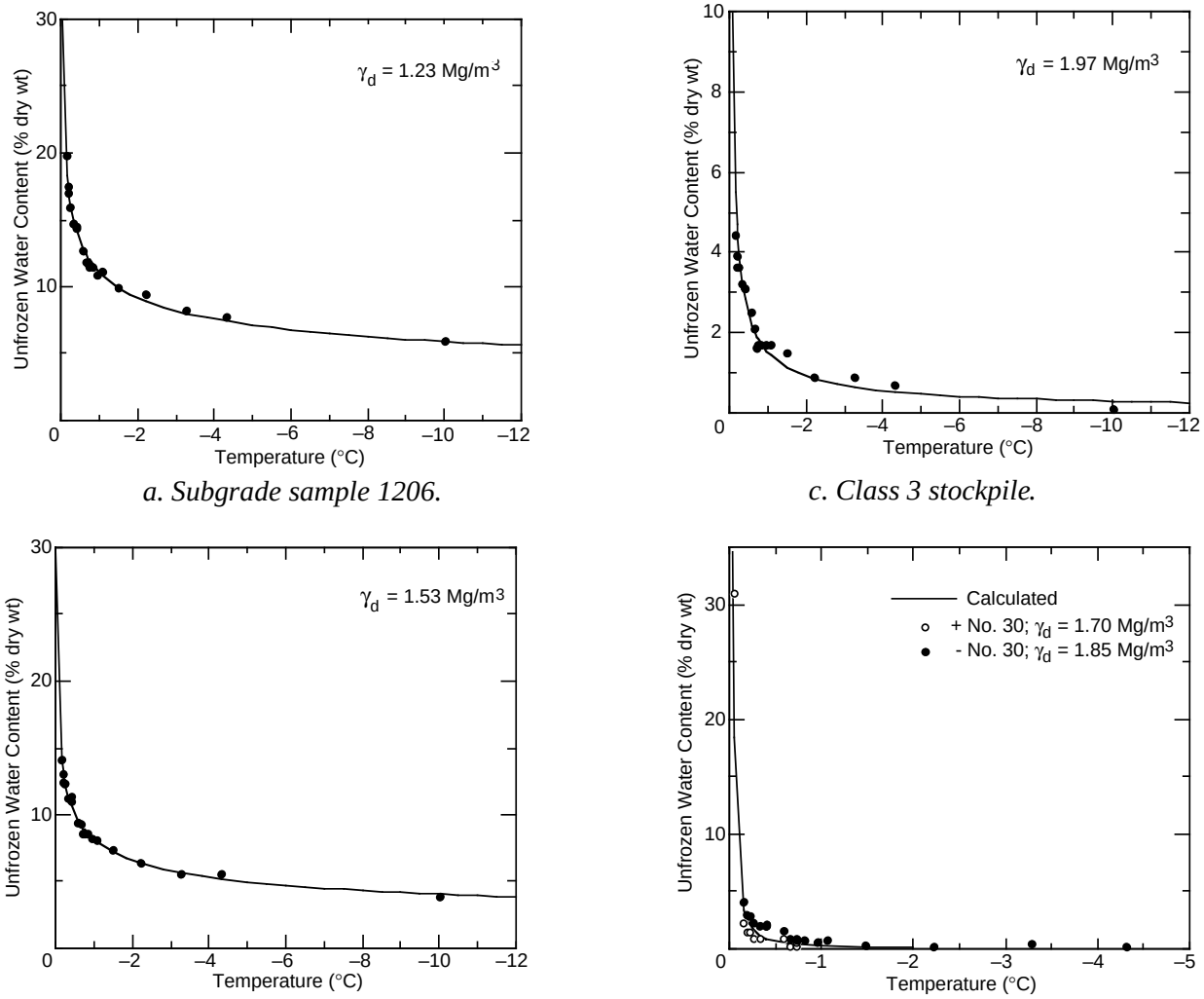

a. Subgrade sample 1206.

c. Class 3 stockpile.

b. Subgrade sample 1232.

d. Class 6 stockpile.

Figure 13. Temperature vs. gravimetric unfrozen water content curves. Solid lines represent calculated values used in the modeling.

the mechanistic procedure, produced with an equation in the form:

$$w_{u-g} = \alpha\left(\frac{-T}{T_0}\right)^{\beta};\ T < 0°C \qquad (4)$$

where w_{u-g} = gravimetric unfrozen moisture content, %
T = temperature, °C
T_0 = 1.0°C
α, β = constants.

Table 9 contains the constants determined for each sample. Additional details about the procedure and test results are in Bigl and Berg (1996a).

Resilient modulus

Laboratory resilient modulus tests were conducted using repeated-load triaxial test procedures, the full details of which are described in Berg et al. (1996) and in Cole et al. (1986, 1987). The tests involve applying a confining pressure to a cylindrical specimen within a cell, while subjecting the specimen to cyclical loading of a deviator stress.

Test procedures—Mn/ROAD materials

The materials tested included the two extreme gradations of base—class 6 special and class 3 special, and the 1206 and 1232 subgrade samples that represent, respectively, the high- and low-heav-

ing subgrades. Specimens of the base materials and subgrade were tested in a frozen saturated condition at three temperatures. The same base material specimens were subsequently warmed to above freezing and tested again at several moisture contents created by drawing a suction at the base of the specimens. To obtain unfrozen data for the subgrade materials, different specimens, referred to as "never frozen," were molded to specific moisture conditions and tested at room temperature.

The specimen size used for the subgrades and the class 3 subbase was 5.1 cm (2 in.) diameter and 12.7 cm (5 in.) long. The coarser class 6 material was tested using specimens measuring 15.2 cm (6 in.) in diameter and 39.4 cm (15.5 in.) in length.

Specimens tested in the frozen/thawed conditions were first molded at the specified moisture/density, which was usually at optimum as determined from the compaction testing. To approximate field conditions, subgrade specimens received a compaction effort of 575 kJ/m^3 (12,000 ft-lb/ ft^3), while class 3 and class 6 special bases were compacted with an effort equal to 2,630 kJ/m^3 (55,00 ft-lb/ ft^3) (Table 10). The specimens were then frozen from the top downwards in a manner similar to the procedure used in the frost susceptibility test (Chamberlain 1987).

For the 1206 subgrade, the "never frozen" specimens were prepared at 3 compactive efforts, with moisture contents intended to be at optimum, 2% above optimum, and 2% below optimum (Table 10).

Table 11a illustrates the sequence of stress conditions applied to the unfrozen specimens, whether thawed or never frozen. We applied only the stress combinations that would avoid excessive permanent strains in the specimens (5% decrease in axial length), depending on the moisture condition and estimated available strength. The frozen specimens were tested holding the confining pressure constant at 69 kPa(10 lb/in.^{2}) and varying the deviator stress (Table 11b). The cyclical deviator stress was applied at each test point until the residual axial strain remained a constant value, which occurred at about 70–100 applied cycles.

Test procedures—
previously tested materials

The methods used during the resilient modulus testing of the materials substituted for the class 5 special and class 4 special bases were nearly identical to the methods of this study. Details of the testing procedures for dense graded stone are described in Cole et al. (1986); the procedures for Albany taxiway A subbase are in Cole et al. (1987). Both materials were molded into 15-cm (6-in.) diam. specimens in the laboratory from field samples and then frozen from the top down at 2.5 cm (1 in.) per day with open system freezing. Resilient modulus testing of the substitute materials differed from the procedure used for the Mn/ROAD materials in two ways: 1) the substitute materials were not saturated prior to freezing, and 2) the loading sequence was different (Tables 11 and 12). Neither of these variations is expected to cause significant differences in modulus values.

Data analysis

For each set of applied deviator and confining stresses, we recorded the resilient and permanent axial and radial strains, and thus we can calculate a resilient modulus and a resilient Poisson's ratio. The following data were then tabulated in a spreadsheet: confining stress, deviator stress, resilient axial strain, resilient radial strain, density, and moisture condition or temperature (Berg et al. 1996).

Linear regression analysis was performed on the data from the resilient modulus testing of the Mn/ROAD materials and the substitute materials for class 4 special and class 5 special. Although regression analysis had been performed on the substitute materials for the class 4 and class 5 special subbases, new regression analyses were performed using our current set of governing parameters. In the regression analysis, the resilient modulus was the dependent variable. For the frozen condition, a function of the unfrozen water content was the independent variable; for the thawed/never frozen condition, various forms and combinations of stress, density, and degree of saturation were the independent variables.

The frozen and unfrozen data were analyzed separately. However, the nonlinear form of the equation used to model the resilient modulus was the same in both cases, as given by

$$M_r = K_1 (P)^{K_2} \quad (5)$$

where K_1 and K_2 are constants and P is a governing parameter.

Table 10. Resilient modulus samples tested.

Subgrade 1206			Subgrade 1232		
No.	*Dry density Mg/m³ (lb/ft³)*	*Water content (% by wt)*	*No.*	*Dry density Mg/m³ (lb/ft³)*	*Water content (% by wt)*
Never frozen			**Never frozen**		
5K Compactive effort *			CE 55 Compactive effort		
18A	1.77 (110.3)	13.7	14A	1.76 (109.8)	13.1
18B	1.72 (107.4	15.9	14B	1.78 (111.4)	12.9
18C	1.69 (105.3)	16.1	14C	1.78 (111.4)	13.0
21B	1.70 (106.4)	19.7	15A	1.78 (111.0)	14.4
21C	1.70 (106.1)	17.3	15B	1.77 (110.8)	14.1
			15C	1.79 (112.0)	13.8
22A	1.69 (108.4)	19.0	15D	1.77 (110.3)	14.3
22B	1.73 (108.0)	19.1			
22C	1.74 (108.6)	18.3	16A	1.76 (109.9)	15.7
			16B	1.75 (109.0)	15.7
CE 12 Compactive effort			16C	1.76 (110.0)	15.6
16A	1.69 (105.6)	13.5	16D	1.77 (110.7)	15.5
16B	1.67 (104.4)	14.1			
16C	1.89 (118.1)	14.3	18A	1.75 (109.3)	17.5
			18B	1.75 (109.5)	17.5
18A	1.69 (105.4)	17.4	18C	1.76 (109.9)	17.5
18B	1.71 (106.9)	15.9	18D	1.76 (110.0)	17.2
18C	1.72 (107.3)	15.9			
			S1	1.70 (106.1)	20.5
20A	1.69 (105.8)	18.5	S2	1.68 (104.7)	21.3
20C	1.70 (106.1)	17.8	S3	1.70 (106.3)	20.3
CE 55 Compactive effort			**Frozen/thawed (saturated)**		
13A	1.74 (108.5)	11.0	CE 12 Compactive effort		
13B	1.68 (105.1)	10.6	M4-1A	1.73 (107.8)	18.9
			M4-1B	1.72 (107.5)	18.8
			M4-2A	1.71 (106.6)	19.3
15A	1.88 (117.3)	13.9	M4-2B	1.72 (107.6)	18.3
15B	1.82 (113.9)	13.4			
15C	1.85 (115.7)	13.5			
			M6-1A	1.69 (105.6)	18.9
17A	1.82 (113.9)	14.9	M6-1B	1.72 (107.1)	19.2
17B	1.86 (116.1)	14.9	M6-3A	1.68 (104.7)	19.4
17C	1.84 (114.9)	14.4	M6-3B	1.68 (104.7)	20.2
Frozen/thawed (saturated)					
CE 12 Compactive effort					
M5-1A	1.71 (106.5)	22.6			
M5-1B	1.67 (104.1)	24.1			
M5-2A	1.68 (104.6)	23.4			
M5-2B	1.70 (106.0)	22.8			

* 5K compactive effort = 5,000 ft-lb/ft^3 (239 kJ/m^3) applied in layers similar to the CE 12 and CE 55 test methods.

Table 10 (cont'd). Resilient modulus samples tested.

Class 3 Subbase			Class 6 Base Course		
No.	*Dry density Mg/m³ (lb/ft³)*	*Water content (% by wt)*	*No.*	*Dry density Mg/m³ (lb/ft³)*	*Water content (% by wt)*
Thawed			**Thawed**		
CE 55 Compactive effort			CE 55 Compactive effort		
Class 3-1	2.11 (131.5)	7.2	Class 6-2	2.08 (130.0)	9.6
	2.12 (132.1)	3.3		2.08 (130.0)	6.0
	2.12 (132.3)	0.8			
			Class 6-3	2.06 (128.4)	10.1
Class 3-2R	2.13 (132.7)	5.1		2.06 (128.4)	8.9
	2.12 (132.6)	3.2		2.09 (130.7)	7.3
	2.12 (132.3)	0.8			
			Class 6-4	2.09 (130.6)	9.5
Class 3-3	2.09 (130.4)	8.3		2.09 (130.6)	7.5
	2.10 (131.2)	6.7		2.14 (133.8)	7.2
	2.10 (130.9)	2.1		2.14 (133.8)	6.5
	2.10 (131.4)	1.4			
			Class 6-5	2.06 (128.7)	9.3
Class 3-4	2.08 (129.6)	9.3		2.06 (128.7)	7.1
	2.09 (129.8)	7.9		2.05 (128.2)	5.1
	2.09 (130.5)	4.0		2.05 (128.2)	4.8
	2.10 (131.0)	2.4		2.10 (131.0)	2.4
Frozen			Class 6-6	2.13 (133.1)	8.9
Class 3-1	2.06 (128.3)	7.6		2.18 (136.0)	4.9
Class 3-2	2.09 (130.7)	6.2		2.18 (136.0)	4.4
Class 3-3	2.03 (126.5)	9.3		2.14 (133.3)	1.6
Class 3-4	2.02 (125.8)	10.1		2.14 (133.8)	0.7
			Class 6-9	2.10 (134.2)	8.2
				2.08 (136.2)	7.0
				2.06 (136.2)	6.1
				2.09 (136.2)	5.4
				2.17 (135.3)	4.0
				2.17 (135.3)	1.4
				2.18 (136.3)	0.5
			Frozen		
			Class 6-1	2.10 (130.9)	9.4
			Class 6-2	2.08 (130.0)	9.6
			Class 6-3	2.06 (128.4)	10.1
			Class 6-4	2.09 (130.6)	9.5
			Class 6-6	2.13 (133.1)	8.9
			Class 6-9	2.15 (134.2)	8.2

Frozen. In attempting to represent the frozen data with the general form eq 5, we tried three different governing parameters, all related to the unfrozen water content of the material, w_u. The unfrozen water content expressed in gravimetric form, w_{u-g}, was determined as part of this study (eq 4). The α and β constants characteristic of each material are listed in Table 9.

The first governing parameter we tried was w_{u-g}, expressed as a decimal, which had been normalized to the total gravimetric water content in the sample, w_t, expressed as a decimal, also. The

Table 11. Stress conditions of resilient modulus tests in current study.

Confining pressure σ_3, *kPa (lb/in.^{2})*	*Deviator stress* σ_d, *kPa (lb/in.^{2})*	*Stress ratio* (σ_1/σ_3)
a. Thawed or never-frozen specimens		
48.3 (7.0)	48.3 (7.0)	2.0
48.3 (7.0)	34.5 (5.0)	1.7
48.3 (7.0)	27.6 (4.0)	1.6
48.3 (7.0)	20.7 (3.0)	1.4
48.3 (7.0)	13.8 (2.0)	1.3
48.3 (7.0)	6.9 (1.0)	1.1
48.3 (7.0)	3.4 (0.5)	1.1
27.6 (4.0)	48.3 (7.0)	2.8
27.6 (4.0)	34.5 (5.0)	2.3
27.6 (4.0)	27.6 (4.0)	2.0
27.6 (4.0)	20.7 (3.0)	1.8
27.6 (4.0)	13.8 (2.0)	1.5
27.6 (4.0)	6.9 (1.0)	1.3
27.6 (4.0)	3.4 (0.5)	1.1
13.8 (2.0)	34.5 (5.0)	3.5
13.8 (2.0)	27.6 (4.0)	3.0
13.8 (2.0)	20.7 (3.0)	2.5
13.8 (2.0)	13.8 (2.0)	2.0
13.8 (2.0)	6.9 (1.0)	1. 5
13.8 (2.0)	3.4 (0.5)	1.3
6.9 (1.0)	34.5 (5.0)	6.0
6.9 (1.0)	27.6 (4.0)	5.0
6.9 (1.0)	20.7 (3.0)	4.0
6.9 (1.0)	13.8 (2.0)	3.0
6.9 (1.0)	6.9 (1.0)	2.0
6.9 (1.0)	3.4 (0.5)	1.5
b. Frozen specimens		
69 (10)	34 (5)	–
69 (10)	69 (10)	–
69 (10)	103 (15)	–
69 (10)	138 (20)	–
69 (10)	207 (30)	–
69 (10)	276 (40)	–
69 (10)	345 (50)	–
69 (10)	483 (70)	–
69 (10)	621 (90)	–
69 (10)	690 (100)	–

Notes:

Thawed samples: each combination of stresses normally used at each moisture condition.

Frozen samples: each combination of stresses normally used at each of three temperatures.

Table 12. Stress conditions of resilient modulus tests—previous study.

Confining pressure $\sigma_{3,}$, *kPa (lb/in.^{2})*	*Deviator stress* $\sigma_{d,}$, *kPa (lb/in.^{2})*	*Stress ratio* (σ_1/σ_3)
a. Thawed specimens		
6.9 (1.0)	3.4 (0.5)	1.5
13.8 (2.0)	6.9 (1.0)	1.5
27.6 (4.0)	13.8 (2.0)	1.5
48.3 (7.0)	24.1 (3.5)	1.5
69.0 (10.0)	34.5 (5.0)	1.5
6.9 (1.0)	6.9 (1.0)	2.0
13.8 (2.0)	13.8 (2.0)	2.0
27.6 (4.0)	27.6 (4.0)	2.0
48.3 (7.0)	48.3 (7.0)	2.0
69.0 (10.0)	69.0 (10.0)	2.0
6.9 (1.0)	10.3 (1.5)	2.5
13.8 (2.0)	20.7 (3.0)	2.5
27.6 (4.0)	41.4 (6.0)	2.5
48.3 (7.0)	72.4 (10.0)	2.5
69.0 (10.0)	103.4 (15.0)	2.5
b. Frozen specimens		
6.9 (10)	60 (9)	–
6.9 (10)	138 (20)	–
6.9 (10)	207 (30)	–
6.9 (10)	276 (40)	–
6.9 (10)	345 (50)	–
6.9 (10)	483 (70)	–
6.9 (10)	621 (90)	–
6.9 (10)	827 (120)	–

resulting equation was as follows:

$$M_r = K_1(w_{u-g} / w_t)^{K_2}. \quad (6)$$

This governing parameter has a good physical basis. When the material is very cold and solidly frozen, there is very little unfrozen water and the ratio w_{u-g}/w_t is a small number, << 1; and when the material is just below the freezing point, w_{u-g}/w_t approaches a value of 1. When this form of the equation was used in the mechanistic design procedure (Bigl and Berg 199b), the calculated amount of total water was often very high, and the ratio of unfrozen water to total water was unreasonably small. Therefore, other relationships were considered.

The final two forms that were used to represent the unfrozen water content in the governing pa-

rameter of eq 5 were directly related to the unfrozen water content, as follows: 1) w_{u-g}, expressed as a decimal, normalized to a unit unfrozen water content, w_0, of 1.0 (i.e., as calculated with eq 4); and 2) the volumetric unfrozen water content, w_{u-v}, expressed as a decimal, normalized to a unit unfrozen water content, w_0, of 1.0. The volumetric unfrozen water content was determined with the equation:

$$w_{u-v} = w_{u-g}\,\gamma_d \tag{7}$$

where γ_d = dry density, Mg/m^3. The resulting equations with these terms substituted as the governing parameter were:

$$M_r = K_1(w_{u-g} / w_0)^{K_2} \tag{8}$$

and

$$M_r = K_1(w_{u-v} / w_0)^{K_2} \tag{9}$$

In analyzing the frozen resilient modulus data, the value of the governing parameter (w_{u-g}/w_t, w_{u-g}/w_0, w_{u-g}/w_0) at each test point was determined from the temperature (and total water content, if necessary). Then, regression analysis was conducted to determine the relationship between these values and the measured resilient modulus. Data from the thawed, undrained state (assigned to be at a temperature just barely below freezing) were analyzed along with the frozen data. Regression analysis was then conducted to determine the relationship between these values and the measured resilient modulus (Table 1a).

The left-hand graphs in Figure 14 compare the frozen resilient modulus data (solid circles) with predictions from the regression equations with the three different governing parameters. The figure shows that the frozen modulus does vary primarily as a function of the unfrozen water content. A minor amount of variation results from the various stress combinations acting on the specimens, as shown from the vertical spread in the data at any particular temperature. The predictive equations without normalization to total water appear to pass nearer to the center of the range of data collected at temperatures warmer than –2.0°C.

Thawed/never frozen. To analyze data from the thawed or never frozen specimens, the governing parameter in the general form equation (eq 5) was set to be a stress function. The constant K_1 was considered to be a function of the moisture level expressed as the degree of saturation in the sample and, when a range of data were available, the dry density. Thus, the general equation becomes

$$M_r = K_1[f(\sigma)]^{K_2} \tag{10}$$

which includes the term

$$K_1 = C_0(S / S_0)^{C_1} \tag{11}$$

or

$$K_1 = C_0(S / S_0)^{C_1}(\gamma_d / \gamma_o)^{C_2} \tag{12}$$

where $f(\sigma)$ = a stress parameter normalized to a unit stress of 6.9 kPa (1.0 lb/ft^2)
C_0, C_1, C_2 = constants
S = the degree of saturation (%)
S_0 = a unit saturation (1.0 %)
γ_o = a unit density (1.0 Mg/m^3).

Three stress parameters were investigated to help characterize the stress dependence of the materials tested. These included J_1, the bulk stress (or first stress invariant); t_{oct}, the octahedral shear stress; and J_2/τ_{oct}, the ratio of the second stress invariant to the octahedral shear stress. In our repeated-load triaxial test, where $s_2 = s_3$ and $s_1 = s_3 + s_d$, the functions are given as:

$$J_1 = 3\sigma_3 + \sigma_d$$

$$\tau_{oct} = \frac{\sqrt{2}}{3}\sigma_d$$

and

$$J_2 / \tau_{oct} = \frac{9\sigma_3^2 + 6\sigma_3\sigma_d}{\sqrt{2}\sigma_d}$$

where

$$J_1 = \sigma_1 + \sigma_2 + \sigma_3$$

$$J_2 = \sigma_1\sigma_2 + \sigma_2\sigma_3 + \sigma_1\sigma_3$$

$$\tau_{oct} = \tfrac{1}{2}\sqrt{(\sigma_1 - \sigma_2)^2 + (\sigma_2 - \sigma_3)^2 (\sigma_1 - \sigma_3)^2}\,.$$

We found that the bulk stress parameter, J_1, provided the best fit to the data for the class 6 base material; the ratio J_2/t_{oct} best fit the data of the three subbases: class 3, class 4, and class 5; and t_{oct} best characterized the clay subgrades (Table 1b).

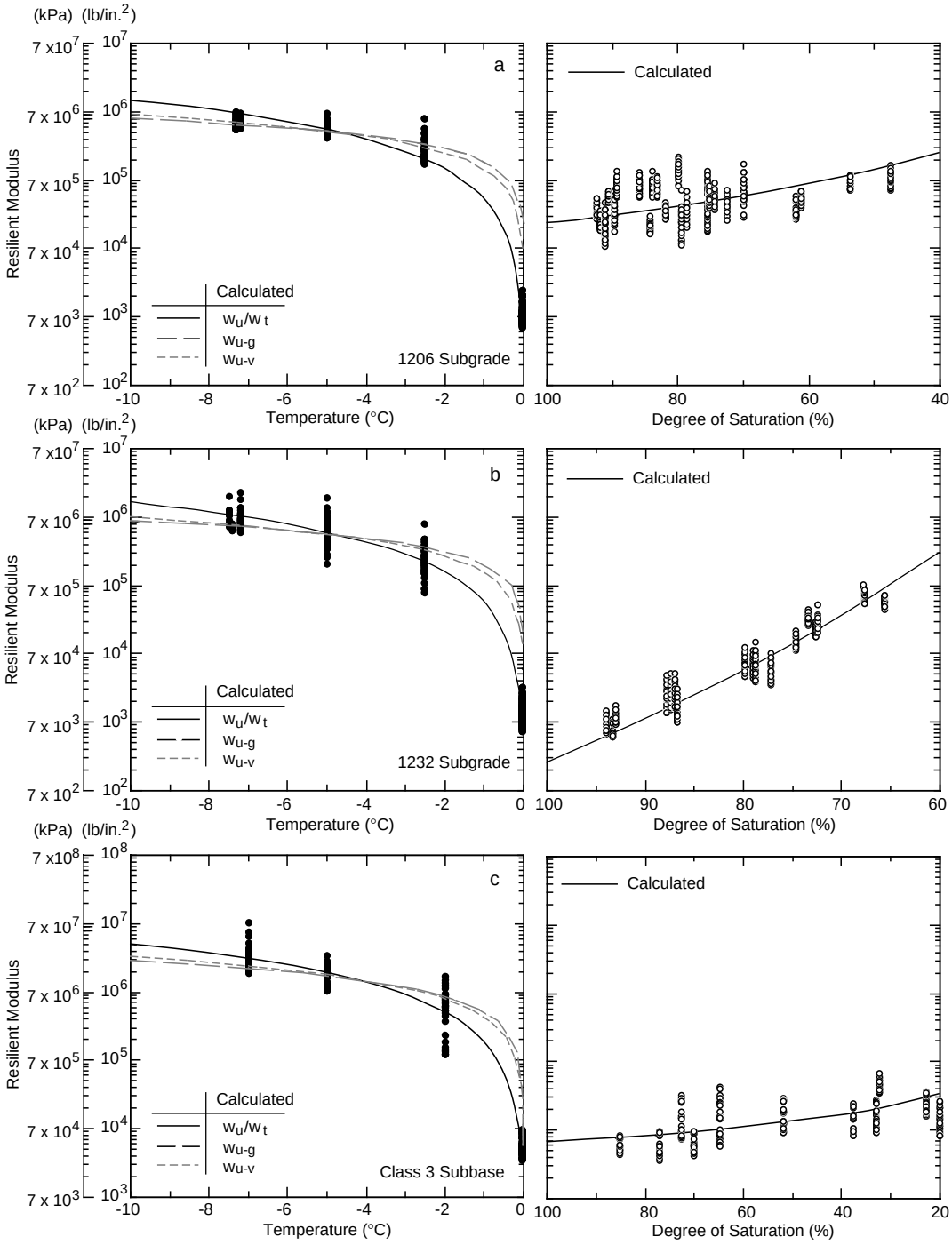

Figure 14. Frozen and unfrozen modulus data compared with calculated moduli from predictive equations.

We also analyzed the data from the class 6 base material in the thawed condition using an equation in the semilog form:

$$M_r = K_1 e^{K_2[f(\sigma)]} \quad (13)$$

As before, K_1 was considered to be a function of the degree of saturation and the dry density (eq 12). In this case, the stress parameter, $f(\sigma)$ was the normalized bulk stress, J_1. This form of the equation was able to accommodate negative stress values that were generated in the layered elastic analysis portion of the predictive model.

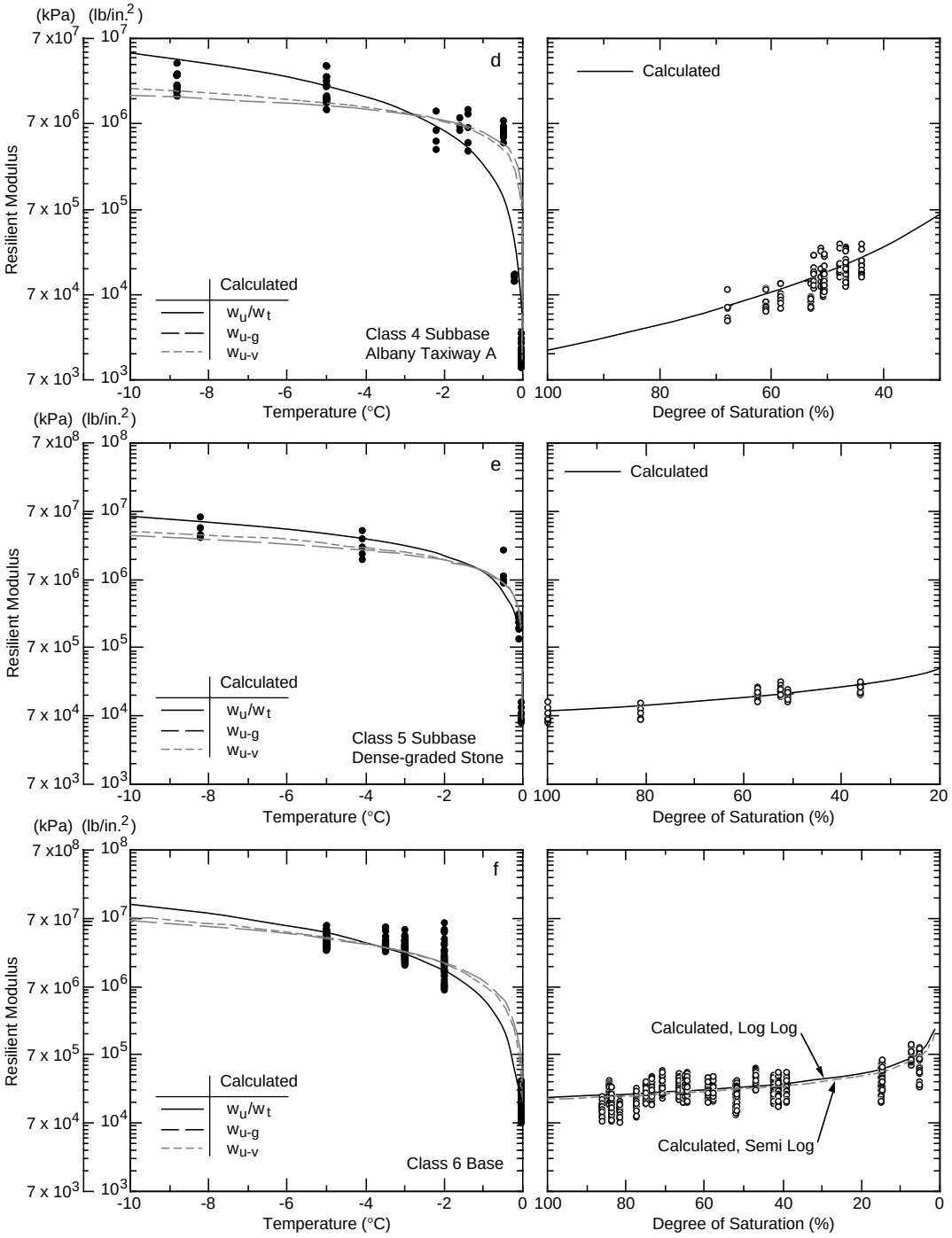

Figure 14 (cont'd). Frozen and unfrozen modulus data compared with calculated moduli from predictive equations.

The right-hand graphs in Figure 14 show the resilient modulus data vs. degree of saturation for the unfrozen specimens. For the two subgrade materials, data are from specimens that were never frozen; data from the base materials are from specimens that were thawed subsequent to freezing. Also shown is a line representing the predicted resilient moduli resulting from the equations given in Table 1, at the mean stress level tested. Where dry density is included in the equation, it was set at the average value of all specimens tested. It can be seen in Figure 14 that moisture level does in-

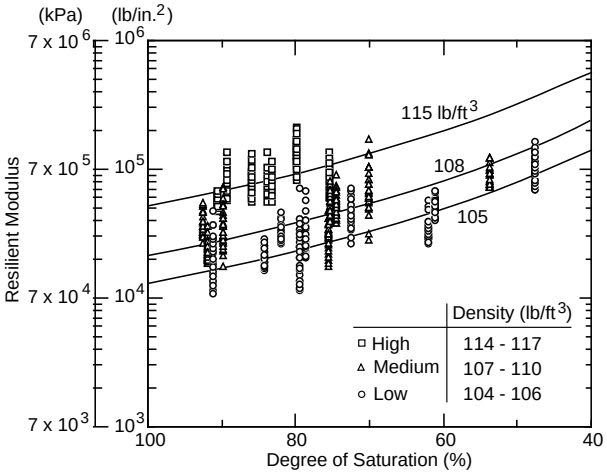

Figure 15. Resilient modulus of never-frozen 1206 subgrade material vs. degree of saturation illustrating the effect of dry density.

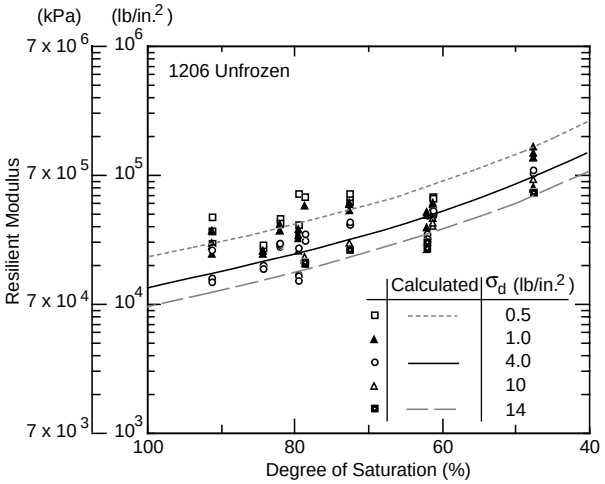

a. Low-density (104–106 lb/ft^3) 1206 subgrade. (The data in this figure are probably in error—see text.)

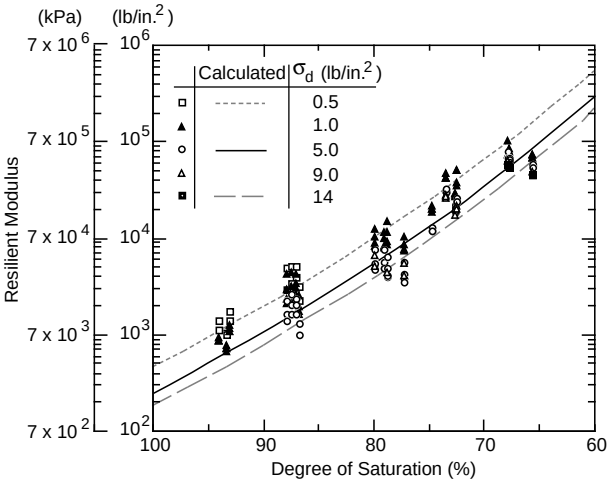

b. 1232 subgrade.

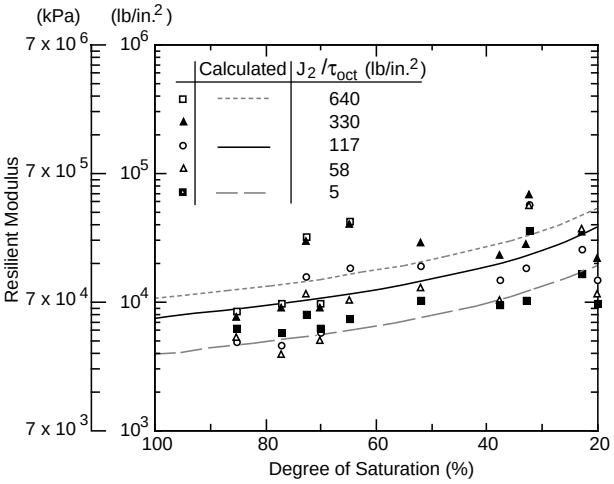

c. Class 3 subbase.

Figure 16. Resilient modulus vs. degree of saturation illustrating effect of stress parameters.

fluence the unfrozen moduli, but to different degrees, depending on the material. The vertical spread in the data points at a particular degree of saturation is the result of the material's response to the different stress combinations applied (Table 11a). In the case of the 1206 subgrade and the class 6 base, it also relates to the variation in density.

To show the influence of density in the 1206 subgrade data, Figure 15 differentiates the data from three density ranges (high, medium, and low), along with the corresponding predicted moduli lines.

The effect of stress combinations is shown in Figure 16 for the low-density 1206 subgrade data, and all of the 1232 subgrade and class 3 special data. The two subgrades display an inverse relationship between modulus and deviator stress; the class 3 special has a proportional relationship between modulus and the stress parameter J_2/t_{oct}.

After the resilient modulus testing was completed, we discovered a calibration error in the system used to test the 1206 subgrade in the unfrozen condition; these data are probably in error. Testing the 1206 subgrade in the frozen condition and all testing on the other materials were done with a different system, which passed its calibration checks. Comparing test results from the 1206 subgrade with those from other materials indicates that unfrozen M_r data for the1206 subgrade may be about an order of magnitude too high.

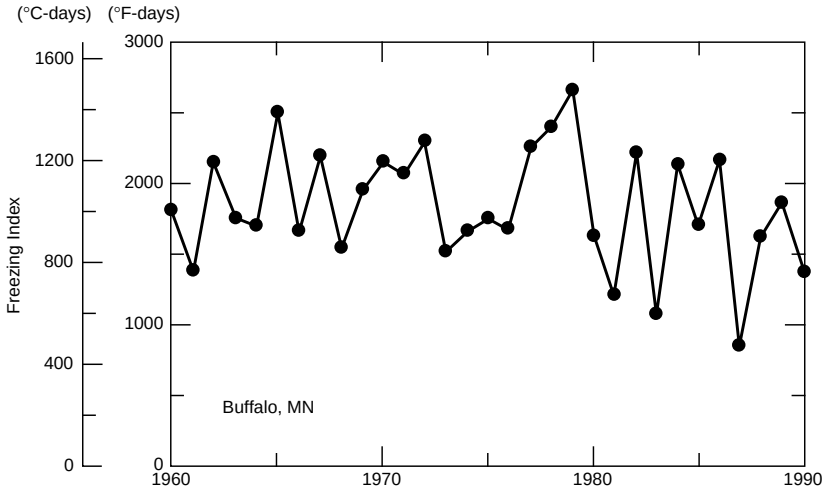

Figure 17. Distribution of seasonal freezing index with time at Buffalo, Minnesota.

PERFORMANCE PREDICTIONS

Performance predictions using the Mechanistic Pavement Design Procedure were conducted in three major efforts:

Phase 1, conducted in the spring of 1991, included an initial simulation series that modeled temperatures from a year close to the mean freezing index. These boundary conditions were applied to eight flexible and three rigid sections.

Phase 2, an effort in the summer of 1992, had two primary objectives. Phase 2A included three series modeling the eight flexible sections with the mean freeze season and changing the method employed to calculate the asphalt and subgrade modulus. Phase 2B investigated the variability in predictions when temperatures from freeze seasons with maximum and minimum freezing indices are applied to a single flexible section.

Phase 3, an effort in the summer of 1993, expanded the investigation of the effects of freeze season characteristics. This series modeled 21 different freeze seasons applied to one full-depth and one conventional flexible section.

Phase 1

Simulation period

Prior to conducting the initial series of simulations, we analyzed the distribution of seasonal air freezing indices (an indication of winter severity) in Buffalo, Minnesota, at a site about 16 km (10 mi) south of Mn/ROAD (Fig. 17). It was decided to simulate the 1959–1960 winter, which had an index very near the average value for the period. The actual days simulated were 1 October 1959 to 14 November 1960, a span of 410 days that allowed some time prior to the start of freezing and included the entire subsequent thaw season.

Pavement sections

The mechanistic pavement design procedure was applied to 11 test sections, which were distributed among the designs as follows: four 5-yr flexible, four 10-yr flexible, two 5-yr concrete, and one 10-yr concrete (Fig. 18). Water table depths were modeled based on field measurements at the site. Seven of the test sections had variable water table depths along their lengths, and these were simulated at the two extreme water table positions. Table 13 lists the test sections and water table conditions simulated as well as the nomenclature used to denote the various cases. The nomenclature includes the Mn/ROAD test section number and the water table depth (in ft) preceded by a "w." For example, f1w9 refers to Mn/ROAD test section ML5-F-1 with a water table 9 ft below the pavement surface and r11w6 refers to section ML10-R-11 with a water table 6 ft below the pavement surface. All but one case involved the high-heaving subgrade (sample 1206) beneath the pave-

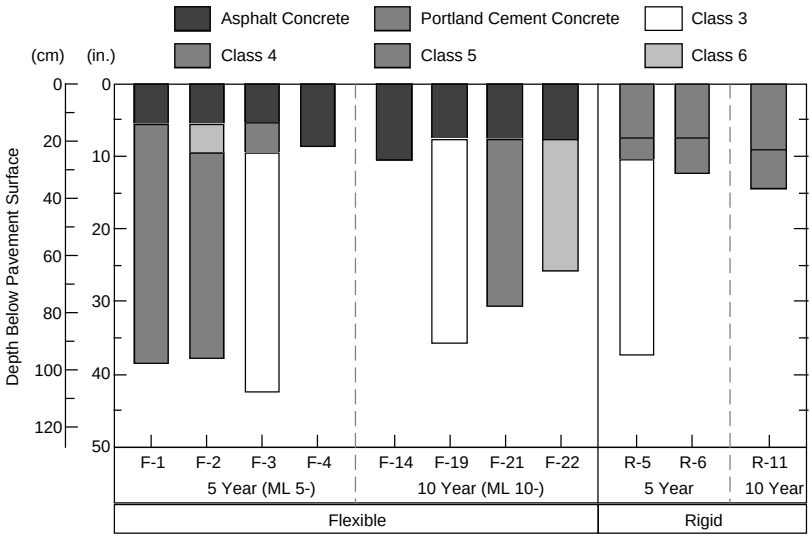

Figure 18. Pavement structure of Mn/ROAD test sections simulated.

Table 13. Test sections simulated, and maximum frost heave/frost penetration preditions.

Mn/ROAD test section	*Simulation cases*	*Water table depth m (ft)*	*Frost heave cm (in.)*	*Frost penetration cm (in.)*
Flexible				
5-year				
ML5-F-1	f1w9	2.7 (9)	0.25 (0.10)	137.9 (54.3)
ML5-F-2	f2w9	2.7 (9)	1.19 (0.47)	121.9 (48.0)
ML5-F-2	f2w20	6.1 (20)	0.33 (0.13)	142.0 (55.9)
ML5-F-3	f3w8	2.4 (8)	0.08 (0.03)	134.1 (52.8)
ML5-F-3	f3w20	6.1 (20)	0.00	142.0 (55.9)
ML5-F-4	f4w6	1.8 (6)	1.37 (0.54)	118.1 (46.5)
ML5-F-4	f4w6 ld	1.8 (6)	1.32 (0.52)	118.1 (46.5)
ML5-F-4	f4w6 ss	1.8 (6)	0.03 (0.01)	137.9 (54.3)
10-year				
ML10-F-14	f14w50	15.3 (50)	0.00	134.1 (52.8)
ML10-F-19	f19w18	5.5 (18)	0.00	142.0 (55.9)
ML10-F-21	f21w18	5.5 (18)	0.00	134.1 (52.8)
ML10-F-21	f21w45	13.7 (45)	0.00	134.1 (52.8)
ML10-F-22	f22w45	13.7 (45)	0.00	134.1 (52.8)
Rigid				
5-year				
ML5-R-5	r5w6	1.8 (6)	1.04 (0.41)	121.9 (48.0)
ML5-R-5	r5w12	3.7 (12)	0.00	137.9 (54.3)
ML5-R-6	r6w4	1.2 (4)	4.72 (1.86)	103.9 (40.9)
ML5-R-6	r6w12	3.7 (12)	0.00	134.1 (52.8)
10-year				
ML10-R-11	r11w6	1.8 (6)	1.42 (0.56)	118.1 (46.5)
ML10-R-11	r11w12	3.7 (12)	0.00	134.1 (52.8)

ld = low density (1.69 Mg/m^3 or 105.5 lb/ft^3)
ss = second subgrade (1232)

Table 14. Material parameters input to FROST for Mn/ROAD test section simulations.

Parameter		*Asphalt*	*PCC Concrete*	*Class 6*	*DGS Class 5*	*TAS Class 4*	*Class 3*	*1206 Subgrade*	*1232 Subgrade*
Soil density (g/cm^3)		2.3	2.3	2.09	1.89	2.16	2.11	1.89	1.99
Specific heat of soil (cal/g °C)		0.2	0.2	0.2	0.2	0.2	0.2	0.2	0.2
Thermal cond. of soil (cal/cm hr °C)		17.5	17.5	17.0	17.0	17.0	17.0	17.0	17.0
Soil porosity (cm^3/cm^3)		0.14	0.14	0.331	0.337	0.206	0.251	0.374	0.320
Soil water characteristics:	A_w	0.3090	0.3090	1.0001	0.4961	0.152	0.1735	0.00240	0.00226
	α	0.3190	0.3190	0.4444	0.3660	0.269	0.3239	0.7134	0.6790
Residual water content (cm^3/cm^3)		0.039	0.039	0.01614	0.05008	0.10741	0.09994	0.2916	0.2638
Saturated hydraulic cond. (cm/hr)		2.10	1.05	6.0	5.54	2.8	4.5	0.14	0.0087
Permeability characteristics:	A_k	0.0349	0.0349	3.723×10^{-8}	3.912	6.58×10^{-5}	1647.1	0.000571	0.001886
	β	2.6450	2.6450	5.6733	1.3930	2.962	0.7207	2.6395	1.8129

ment structure. The final simulation included the lower-heaving subgrade (sample 1232) under the 5-yr full-depth section (ML5-F-4), termed case f4w6ss, or "second subgrade." One of the 1206 subgrade simulations, also the 5-yr full depth section (case f4w6ld) used a lower dry density of 1.69 Mg/m^3 (105.5 lb/ft^3) for the subgrade, as compared with what was set as the "normal" case, or 1.89 Mg/m^3 (118 lb/ft^3).

Material properties

Material properties input to the FROST program are shown in Table 14. Note that the class 3 special, class 6 special, and two subgrade materials were tested as part of this study to determine the information for input to the model. The class 4 special and class 5 special materials were not tested, and their behavior was approximated using data from previously tested materials that most closely matched their specified size gradations. A subbase from taxiway A at the Albany, New York, airport most closely matched the class 4 special subbase specifications; and a dense-graded stone, from Winchendon, Massachusetts, most closely matched the class 5 special material.

In this initial modeling series, the equations used in TRANSFORM to calculate the modulus of base, subbase, and subgrade materials were the gravimetric form of the frozen equations (Table 1a) and the unfrozen equations in Table 1b. For the class 6 special material, we used the semilog form listed in Table 1b. The asphalt concrete modulus was calculated with the Schmidt (1975) relationship.

As stated earlier, after these Phase 1 simulations were completed, we discovered that resilient modulus tests on the 1206 subgrade in the unfrozen condition were probably in error due to a miscalibrated testing system. As a result, the unfrozen subgrade moduli predicted in Phase 1 modeling are likely to be substantially higher than exist in the field, resulting in less damage than would have been obtained with more reasonable moduli.

In the NELAPAV program, we used the linear model for paving materials, and for the base, subbase, and subgrade when frozen. Nonlinear models of various forms (Table 2) were assigned to unfrozen base, subbase, and subgrade as follows: Model 1 (modified to semilog form)—class 6; Model 3—class 3 and class 4; and Model 4—both clay subgrades.

In all of these simulations, it was assumed that the pavement properties were constant from one pavement test section to another. Some of the test sections will possess properties different from others because of the experimental design of the paved surface. Some variations in the asphalt pavement properties could be considered in subsequent modeling efforts, but we maintained the same asphalt pavement properties in all of these simulations.

Results—flexible sections

Figure 19 is an example of output from FROST for the 5-yr full depth simulation (f4w6). The top graph shows the daily mean air temperature for the period from 1 October 1959 to 14 November 1960. The center portion illustrates the predicted frost heave and the bottom graph contains the predicted frost and thaw penetration as functions of time. Frost output graphs for all the flexible cases are compiled in Bigl and Berg (1996b). The freeze season simulated was characterized by several short freeze-thaw events early in the season, followed by a continuous severe freeze event with a fairly rapid spring thaw. Table 13 contains maximum frost heave and maximum frost penetration depths for each of the cases simulated. Simulations with shallower water table depths had greater amounts of heave and less frost penetration compared to simulations with a deeper water table location. Sections that included the substitute for the class 4 special subbase (taxiway A subbase) had higher amounts of heave than those with other combinations of subbase materials.

Figure 20 presents the moduli being calculated by TRANSFORM and passed as seed moduli to NELAPAV for the f4w6 case. The plotted moduli are the minimum values for each day, with the subgrade (top) being located within 0.3 m (1 ft) of the asphalt and subgrade (bottom) being the rest of the modeled section. Note that the predicted asphalt moduli during the summer months are smaller than those of the subgrade, which results in high horizontal strains at the base of the asphalt layer during the summer months. In later simulations of this study, we used another model for predicting asphalt modulus at temperatures above 1°C.

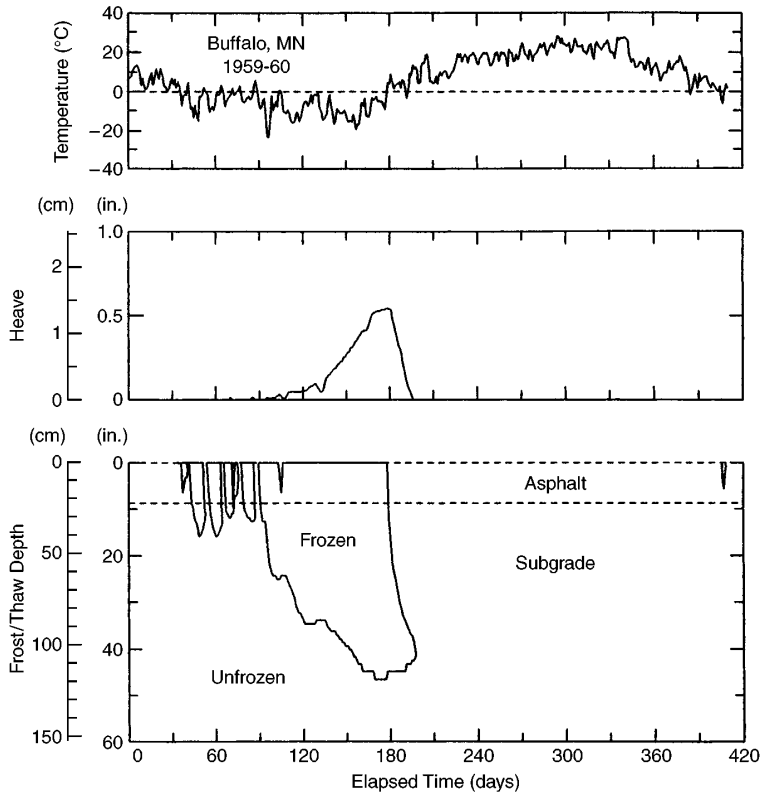

Figure 19. Example output from FROST for Mn/ROAD test section ML5-F4 with a 1.8-m (6-ft) water table. Simulation starts on 1 October.

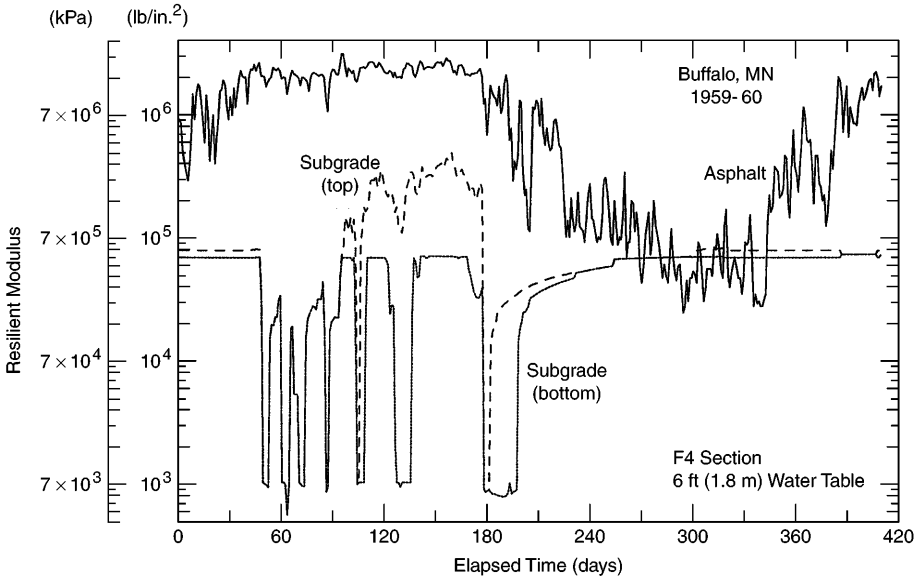

Figure 20. Seed moduli output by TRANSFORM for Mn/ROAD test section ML5-F4 with a 1.8-m (6-ft) water table. Subgrade (top) is within the upper 0.3 m (1 ft) of subgrade beneath the asphalt. Subgrade (bottom) is beneath that layer to the bottom of the modeled section.

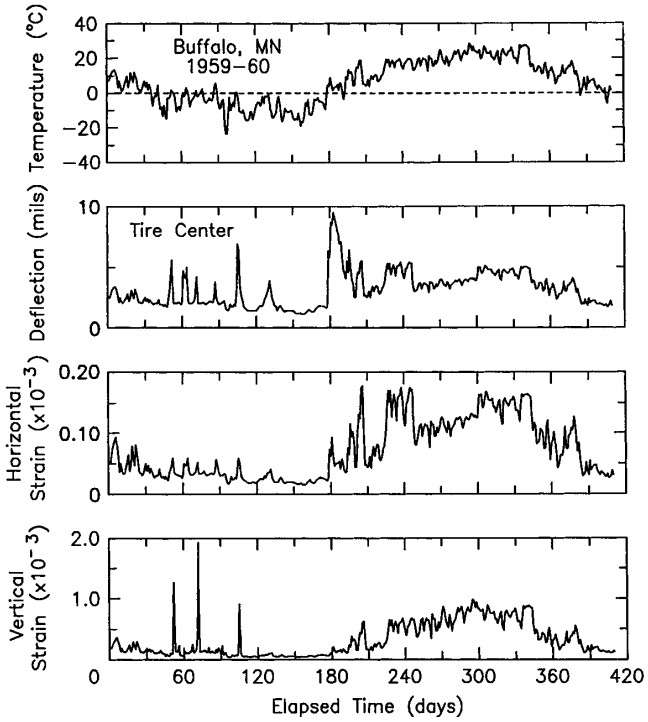

Figure 21. Deflection and strain calculated by NELAPAV for Mn/ROAD test section ML5-F4 with a 1.8-m (6-ft) water table. Horizontal strain is at the base of the pavement. Vertical strain is at the top of the subgrade.

Figure 21 shows the deflection and strains computed by NELAPAV for the f4w6 case. The horizontal strain at the base of the asphalt is small through the winter with a few small peaks during short-term thawing periods. It then exhibits high peaks during spring thaw and summer. It appears to be closely related to the asphalt temperature/modulus during the spring thaw. The vertical strain at the top of the subgrade is also low during the winter with three sharp peaks during thaw events. The vertical strain also rises during spring and summer, closely tracking the pavement surface temperature. The deflection plotted is from the base of the asphalt, but is assumed to be similar to the surface deflection. It also shows peaks during midwinter thaws, and a maximum peak during spring thaw prior to drainage of excess subsurface moisture. Generally, deflections in the summer are greater than winter values.

Table 15 lists the applications to failure predicted from the 1-yr simulation period applied to the flexible sections. The values listed in Table 15 were determined by taking the reciprocal of the one year (365-day) cumulative damage

Table 15. Predicted applications to failure (×1000) from Phase 1 simulation series of flexible pavement test sections.

	Horizontal criteria				*Vertical criteria*		
Cases	*Asp. Inst. MS-1*	*Asp. Inst. MS-11*	*Corps of Engineers*	*Coetzee/ Connor*	*Asp. Inst. MS-1*	*Corps of Engineers*	*FAA*
5-Year							
F1W9	86	498	88	4,380	136,942	5,653	11,879
F2W9	522	1,244	550	42,703	32,477	1,345	1,526
F2W20	722	1,534	764	66,450	155,909	8,226	9,855
F3W8	957	1,706	958	92,419	116,287	2,653	9,611
F3W20	1,068	1,801	1,055	105,202	222,462	7,889	20,632
F4W6	28,585	75,751	90,926	$>10^7$	3,715	15	152
F4W6ld	1,905	20,209	7,036	$>10^7$	165	$>10^7$	$>10^7$
F4W6ss	72	1,180	96	$>10^7$	$>10^7$	$>10^7$	$>10^7$
10-Year							
F14W50	103,272	485,198	605,194	$> 10^7$	8,602	10	251
F19W18	396	6,148	966	75,751	2,962,263	56,680	457,585
F21W18	3,394	30,456	12,751	2,010,107	562,830	84,382	42,478
F21W45	3,404	30,358	12,794	2,010,107	611,772	92,571	48,188
F22W45	7,614	57,315	31,147	8,040,429	73,190	22,415	3,388

Notes:
ld = low density (1.69 Mg/m^3 or 105.5 lb/ft^3)
ss = second subgrade (1232)
Traffic simulated at rate of 562,830 ESAL applications/yr.

value produced by the CUMDAM program and multiplying by the number of applications received by the sections during that time period (562,830 per year). This application rate was based on an initial estimate that the traffic across the test sections would be 2,815,000 ESALs in five years, or 5,630,000 ESALs in 10 years. Subsequent to conducting the Phase 1 series, a revised estimate is that the 5-yr sections will receive 3,300,000 ESAL applications in five years, (i.e., are designed to fail after 3,300,000 ESAL applications); the 10-yr sections will fail at 6,600,000 ESAL applications.

Individual values listed in Table 15 vary anywhere from very much below to very much above the failure values described. By comparing values horizontally across the table for any case, it can be seen that different models estimate substantially different pavement lives for the same strain conditions.

A close review of the values in Table 15 illustrates a variety of interesting occurrences. Some of them are the following:

1. Cases with Mn/ROAD test section ML5-F-4 that employed the lower density subgrade (f4w6ld) or the 1232 subgrade (f4w6ss) predicted the pavement to fail much more quickly than when the higher (optimum) density 1206 subgrade was used. This is due to the fact that the higher density 1206 subgrade used in most simulations maintained a resilient modulus during the summer months in excess of 276,000 kPa (40,000 lb/in.^{2}), but the modulus values for the same period were about 96,000 kPa (14,000 lb/in.^{2}) for f4w6ld and about 6900 kPa (1000 lb/in.^{2}) for f4w6ss. The "low density" predicted moduli are the closest to the values measured during the summer months with an FWD.

2. Variations in water table position in the same test section result in different predicted lifespans, especially if the water table is less than 3 m (10 ft) deep at one location and more than 6.1 m (20 ft) deep at another. Both the ML5-F-2 and ML5-F-3 test section simulations illustrate a shorter predicted life with a shallow water table depth. For the shallow water table conditions, greater availability of water results in higher thaw weakening (reduced modulus values) in the spring.

3. Most of the sections are predicted to fail due to cracking of the pavement caused by tensile stresses at the bottom of the pavement much before they will fail due to rutting caused by excessive deformation of the subgrade. It is only the simulations of the full-depth sections (ML5-F-4, case f4w6, and ML10-F-14, f14w50) that indicate rutting failures may occur before excessive fatigue cracking.

Figures 22–24 illustrate examples of the relation between accumulating damage and time. Additional plots of heave, frost penetration, and cumulative damage for all the flexible sections are compiled in Bigl and Berg (1996b).

Damage related to the horizontal strain criteria has different patterns with time for different models. Damage predicted by the MS-1 (Asphalt Institute) model has some increase during winter thaw events and during the main spring thaw, but a majority of its increase is in the summer period. Predicted damage from the MS-11 (Witczak) model has a consistent pattern of rising during winter and spring thaw periods, and remaining constant during the summer. The pattern of damage accumulation from the Corps of Engineers model is similar to the MS-1 model, especially when the water table is shallow, causing larger resultant deflections and strains. For simulations with deeper water tables, smaller amounts of damage accumulate during the summer.

Damage from models using the vertical strain criteria follow three general patterns: 1) a sharp

Table 16. Applications to failure (×1000) from simulations of rigid test sections.

Case	*RCON = 650 SCI = 80*	*RCON = 500 SCI = 80*	*RCON = 650 SCI = 90*
5-Year			
R5W6	52,601	507	45,244
R5W12	65,598	605	56,452
R6W4	157,655	1,505	135,622
R6W12	132,120	1,701	113,933
10-Year			
R11W6	$>5.6 \times 10^8$	18,761,000	$>5.6 \times 10^8$
R11W12	$>5.6 \times 10^8$	28,141,500	$>5.6 \times 10^8$

Notes:
RCON = concrete flexural strength, lb/in.^{2}
SCI = surface condition index at failure
Traffic simulated at rate of 562,830 ESAL applications/yr.

rise during spring thaw period with no accumulation at other times of the year (e.g., Fig. 23); 2) a series of increases during winter thaw events and the spring thaw (Fig. 22), and 3) in the cases with lower modulus subgrades, a gradual increase in damage during the spring, with sharper increases in the summer (Fig. 24). This last result is likely due to the anomalously low asphalt moduli being predicted by the Schmidt model.

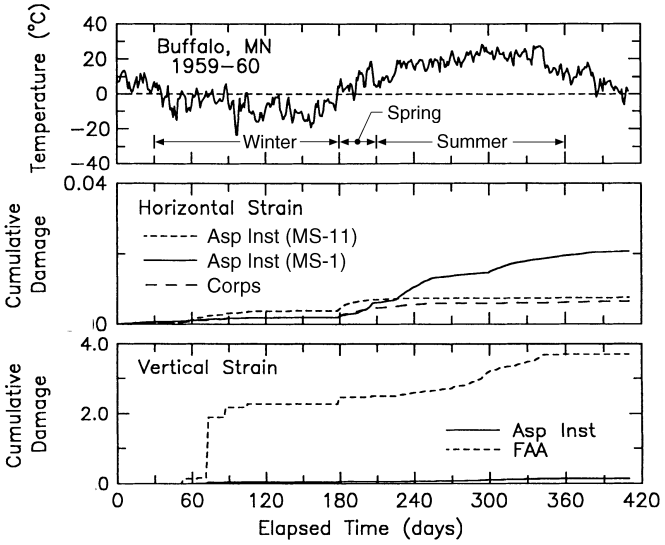

Figure 22. Cumulative damage for case f4w6 with "normal" subgrade.

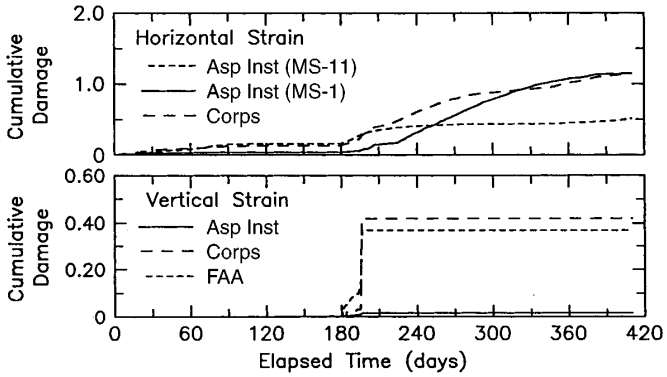

Figure 23. Cumulative damage for case f2w9.

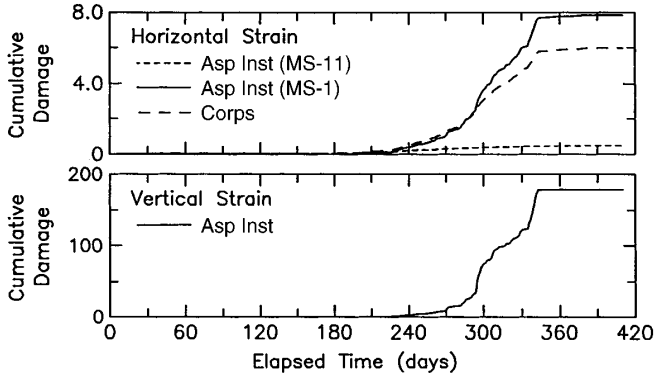

Figure 24. Cumulative damage for case f4w6 with 1232 subgrade.

Results—rigid sections

Predicted application to failure for the concrete sections is shown in Table 16, with the three sections in the table indicating the results of a sensitivity study. In the left-hand section, the flexural strength of the concrete was set at 4480 kPa (650 lb/in.^{2}) and the surface condition index (SCI) at the point of failure was set at 80. In the central section, the flexural strength was reduced to 3448 kPa (500 lb/in.^{2}), while the SCI remained at 80. For predictions in the right-hand columns, the flexural strength was kept at 4480 kPa (650 lb/in.^{2}) and the SCI was increased to 90. A comparison of the cumulative damage with time for the case representing section ML5-R-5 with a 1.8-m (6-ft) water table (r5w6) using all three combinations of flexural strength and SCI is also illustrated in Figure 25. Bigl and Berg (1996b) has a compilation of graphs depicting the frost/thaw penetration and cumulative damage for all rigid sections simulated.

Cases with a flexural strength of 4480 kPa exhibited very little damage, with the ML10-R-11 section having immeasurable damage. Reducing the flexural strength to 3448 kPa increased the predicted damage for the 5-yr sections, but had little effect on damage in the 10-yr section.

The pattern of damage accumulation with time varied with the test section simulated. ML5-R-5 experienced rapid increases in damage during the thaw periods, but also had an equivalent increase in damage over the summer months. The other sections experienced a majority of their damage during the thaw periods and very little damage during the summer.

The low damage predictions result from the fact that the model predicts damage at the center of a slab, whereas the majority of damage occurs at the slab edges. Chou (1989) recommends increasing the stresses computed from the layered elastic method by a factor of 1.33 to estimate the coverage levels for roadway pavements.

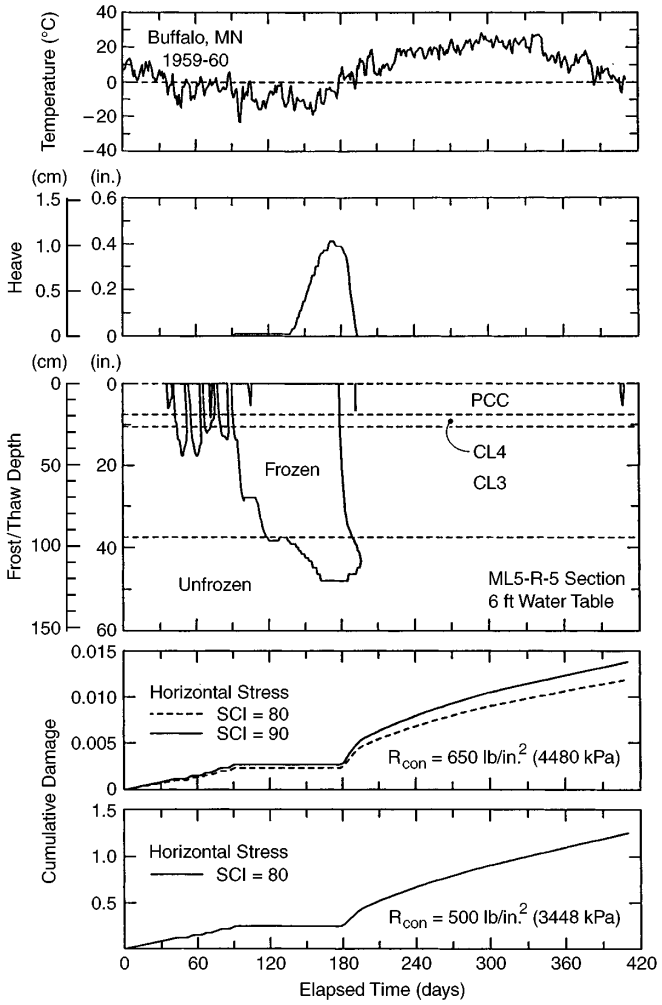

Figure 25. Cumulative damage for case r5w6.

Phase 2A

To address problems discovered in the Phase 1 modeling series, three additional simulation series were conducted on the eight flexible test sections studied in Phase 1 with the water table located at the shallowest position. A change that applied to all three series was that the normalized volumetric unfrozen water content form of the frozen modulus equations (Table 1a), rather than the normalized gravimetric form used in Phase 1.

The first of the new series was essentially a repeat of the initial series in that it used the Schmidt model (Fig. 7) for calculation of the asphalt modulus and the high density 1206 form of the subgrade for modulus calculations. It differed from the initial series in that the normalized volumetric unfrozen water content form of the frozen modulus equations was utilized. A mistake in the CUMDAM program was also remedied—correcting the value of the subgrade modulus used in the Corps of Engineers vertical strain damage calculation. Table 17 lists the results of this series in the rows labeled "Schmidt." In general, predictions of applications to failure in the conventional cross sections were less than in the original series using the horizontal strain criteria and greater using the vertical strain criteria. In the full depth sections (F4 and F14), applications to failure were increased in both the horizontal and vertical strain criteria.

The second series addressed the issue that the Phase 1 simulations computed summer asphalt moduli that were lower than considered reasonable. In this series, the Ullidtz model was used to calculate the asphalt modulus at temperatures greater 1°C; at colder temperatures, the Schmidt model was used (Fig. 7). This series also used the high density 1206 form for the subgrade modulus calculations. Results for this series are shown in Table 17 in rows labeled "Ullidtz." In nearly all cases, this series produced higher predicted applications to failure than the corresponding Schmidt series.

The third series also used the Ullidtz model to calculate the asphalt modulus. In addition, it addressed the problem from the Phase 1 simulations that during the summer the predicted subgrade moduli based on the high-density 1206, or "normal" form were higher than FWD-measured values. For this series, the unfrozen subgrade modulus, when recovered, was set to be constant at 1.03×10^5 kPa (15,000 lb/in.^{2}). This value was chosen as being approximately equal to an average value back-calculated from FWD measurements on subgrade during fall 1991.* As a result of this modulus approximation, the linear model (model 0 in Table 2) was used in NELAPAV for all subgrade calculations. The applications to failure from this series are listed in Table 17 as "Ull-15K." In the conventional sections including a base/subbase, the applications to failure were slightly lower than those resulting from the previous case with the Ullidtz asphalt model and the higher-modulus subgrade;

* D. Van Deusen, Mn/ROAD, person. comm. 1992.

Table 17. Predicted applications to failure (×1000) from simulations of flexible test sections run in Phase 2A series.

		Horizontal criteria				*Vertical criteria*		
Cases		*Asp. Inst. MS-1*	*Asp. Inst. MS-11*	*Corps of Engineers*	*Coetzee/ Connor*	*Asp. Inst. MS-1*	*Corps of Engineers*	*FAA*
5-year								
F1W9	Phase 1	86	498	88	4,380	136,942	5,653	11,879
	Schmidt	85	414	78	3,557	244,709	3,297	15,665
	Ullidtz	651	935	218	17,616	258,179	3,430	17,025
	Ull-15K	617	863	201	15,578	213,193	3,133	18,441
F2W9	Phase 1	522	1,244	550	42,703	32,477	1,345	1,526
	Schmidt	271	859	259	14,634	210,011	2,840	11,389
	Ullidtz	970	1,429	376	37,053	255,832	3,262	15,488
	Ull-15K	908	1,303	340	31,925	117,747	1,971	6,649
F3W8	Phase 1	957	1,706	958	92,419	116,287	2,653	9,611
	Schmidt	533	1,224	487	32,818	96,046	1,197	7,298
	Ullidtz	1,255	1,842	528	58,812	87,260	1,108	6,381
	Ull-15K	1,225	1,705	503	54,327	115,098	1,404	10,501
F4W6	Phase 1	28,585	75,751	90,926	$>10^7$	3,715	15	152
	Schmidt	45,171	121,039	175,884	$>10^7$	4,505	314	164
	Ullidtz	65,218	123,699	149,292	$>10^7$	11,952	317	246
	Ull-15K	7,055	26,561	8,219	3,752,200	7,996	331	467
10-Year								
F14W50	Phase 1	103,272	485,198	605,194	$>10^7$	8,602	10	251
	Schmidt	126,479	721,577	970,397	$>10^7$	11,687	417	336
	Ullidtz	209,230	760,581	852,773	$>10^7$	17,107	412	359
	Ull-15K	19,902	153,779	40,903	$>10^7$	26,943	787	2,232
F19W18	Phase 1	396	6,148	966	75,751	2,962,263	56,680	457,585
	Schmidt	309	4,335	635	43,328	4,329,462	37,175	632,393
	Ullidtz	2,948	14,480	2,278	574,316	4,329,462	37,422	639,580
	Ull-15K	2,688	12,367	1,976	469,025	1,125,660	18,173	264,239
F21W18	Phase 1	3,394	30,456	12,751	2,010,107	562,830	84,382	42,478
	Schmidt	1,958	16,072	4,701	420,022	865,892	10,452	70,442
	Ullidtz	8,515	33,402	9,343	3,752,200	792,718	9,689	61,849
	Ull-15K	6,661	23,335	6,513	2,345,125	457,585	8,752	66,686
F22W45	Phase 1	7,614	57,315	31,147	8,040,429	73,190	22,415	3,388
	Schmidt	1,750	21,507	5,070	493,711	68,388	1,078	3,077
	Ullidtz	8,235	42,964	9,192	3,752,200	85,667	1,278	4,297
	Ull-15K	6,186	26,045	5,986	2,084,556	120,520	2,086	9,840

Notes:

Phase 1—previous work, Schmidt— new series with Schmidt asphalt model, Ullidtz—new series with Ullidtz asphalt model above 1°C, Ull-15K—new series with Ullidtz asphalt model and summer subgrade modulus = 15K lb/in.^{2} Traffic simulated at rate of 562,830 ESAL applications/yr.

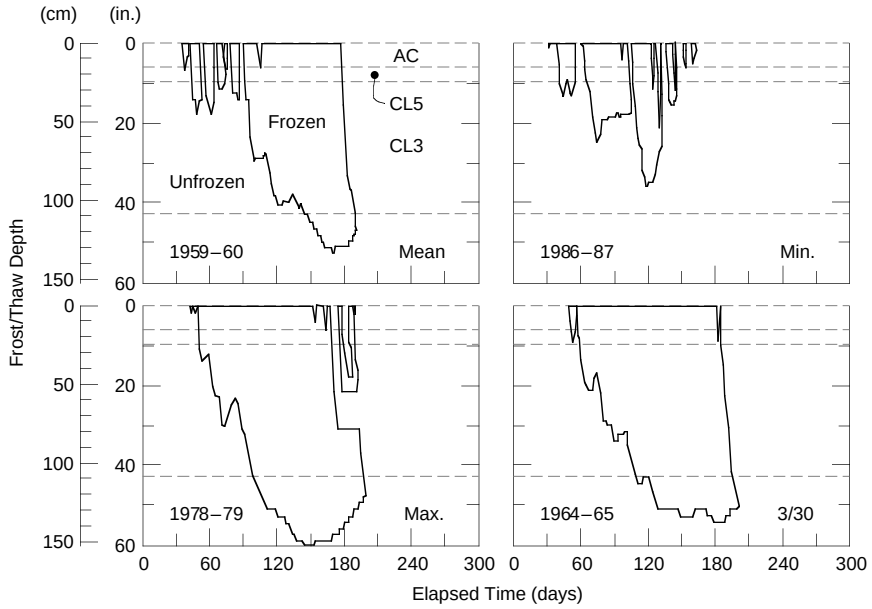

Figure 26. Frost and thaw penetrations predicted by FROST for freeze seasons in Phase 2B environmental sensitivity study. Simulations start on 1 October.

in the full depth sections, they were quite a bit lower.

A comparison of the Ullidtz/15K subgrade series results with the originally designed failure at 3,300,000 applications for the 5-yr sections and at 6,600,000 applications for the 10-yr sections yields the following conclusions:

1. In general, the Mechanistic Pavement Design Procedure predicts the 5-yr conventional sections to fail due to asphalt cracking prior to the end of the design life, while failure from subgrade rutting is predicted beyond the design life.

2. Predictions for the 5-yr full-depth section (F4) indicate that it will not fail from asphalt cracking, but two of the three criteria for subgrade rutting indicate early failure.

3. The two 10-yr conventional sections with class 5 and class 6 special bases (F21 and F22) are predicted to fail from asphalt cracking at about the end of the design applications, while subgrade rutting criteria indicate longer life.

4. The 10-yr conventional section with class 3 special subbase (F19) may fail due to asphalt cracking, but not from subgrade rutting.

5. Predictions for the 10-yr full-depth section (F14) indicate that it will not fail from asphalt cracking, but two of the three criteria for subgrade rutting indicate early failure.

Phase 2B

To investigate the influence of the applied freeze/thaw season on the predicted performance of the sections, an environmental effects sensitivity series was conducted using the single conventional flexible test section, F3, which included class 5 special and class 3 special materials as its base and subbase courses (Fig. 18) and a water table at a depth of 2.4 m (8 ft). Prior simulations had applied upper boundary temperatures from the season with a freezing index near to the 30-yr mean, 1959–60 (freezing index 1003°C-days or 1806 °F-days). This new series applied temperatures from 3 other freeze/thaw seasons, including those with freezing indices equal to the mean of the three coldest seasons during the period 1959 to 1987 and the maximum and minimum for the 1959–1987 period. These seasons were as follows: maximum—1978–79 (1477 °C-days or 2658 °F-days), minimum—1986–87 (4.67 °C-days or 841 °F-days), and mean 3 coldest out of 30—1964–65 (1391 °C-days or 2503 °F-days). Results from these years were compared with f3w8 predictions for the mean year that had been run in the Phase 2A "Schmidt" series, since this Phase 2B series also used the Schmidt model for asphalt modulus calculations and the high density 1206 form for the subgrade modulus calculations.

Figure 26 shows the freeze/thaw penetration in the F3 section predicted by FROST for all four freeze seasons. In the mean year, multiple small freeze/thaw events were followed by a long freeze event that penetrated the subgrade and a spring

Table 18. Performance predictions for F3 test section with water table at 2.4 m (8 ft). Freeze/ thaw seasons applied as upper boundary temperatures were mean year (1959–60), maximum year (1978–79), minimum year (1986–87), average of the 3 coldest out of 30 (1964–65).

	Applications to failure (×1000)			
Failure criteria	*Mean*	*Max*	*Min*	*3/30*
Horizontal				
Asphalt Institute (MS-1)	533	384	573	397
Asphalt Institute (MS-11)	1,224	1,215	1,117	1,445
Corps of Engineers	487	375	593	368
Coetzee/Conner	32,818	25,284	50,660	23,530
Vertical				
Asphalt Institute (MS-1)	96,046	51,120	$>10^7$	96,046
Corps of Engineers	1,197	600	$>10^7$	1,143
FAA	7,298	4,080	$>10^7$	7,625

Note: Traffic simulated at rate of 562,830 ESAL applications/yr.

warming that remained above freezing. The minimum year had several freeze/thaw events, but they were less severe—none of them penetrated beyond the base course materials. The maximum year began with a very severe freeze event that penetrated to the subgrade and lasted all winter. In the spring, thawing of this freeze bulb was interrupted by two smaller freeze events, such that there existed a thawed layer in the subbase between two frozen zones. The year with a freezing index equal to the mean of the three coldest in 30 (3/30 year) had a freeze season consisting of a single severe freeze event that penetrated into the subgrade, which then thawed with no small freeze events.

Table 18 lists the predicted damage in terms of applications to failure from this environmental series, in which traffic was simulated at 562,830 ESALs per year. Compared with the mean year, failure due to the horizontal strain criteria (asphalt cracking) is predicted earlier with the maximum year and the 3/30 year, and later with the minimum year. However, the spread of values is not that great, and three of the four models predict failure sooner than the design figure of 3,300,000 applications for all four of the seasons modeled. Time of failure due to the vertical strain criteria (asphalt rutting) is predicted sooner in the maximum year than the mean year, and at about the same time as the mean year with the 3/30 year. No damage due to subgrade rutting was predicted with the minimum year in which no frost penetrated the subgrade.

Phase 3

The third phase of the study modeled two flexible pavement sections to which 21 years of environmental conditions were applied. Various analyses were conducted attempting to correlate the predicted damage with the characteristics of the freeze seasons simulated.

Cross sections/Material properties

The two cross sections simulated employed layer thicknesses from two Mn/ROAD test sections. The first, section F4, was a "full-depth" section consisting of an asphalt layer lying directly above the lean clay subgrade. The second, section F3, was a "conventional" section, including class 6 special as the base material (substituted for class 5 special in the actual pavement structure) and class 3 special as the subbase.

Physical properties used for the materials were the same as shown in Table 14, with the exception that a lower density (1.69 Mg/m^3, 105.5 lb/ft^3) was used for the 1206 subgrade (Fig. 15). The asphalt modulus was calculated with a combination of the Ullidtz model at above 1°C temperatures and the Schmidt model at colder temperatures.

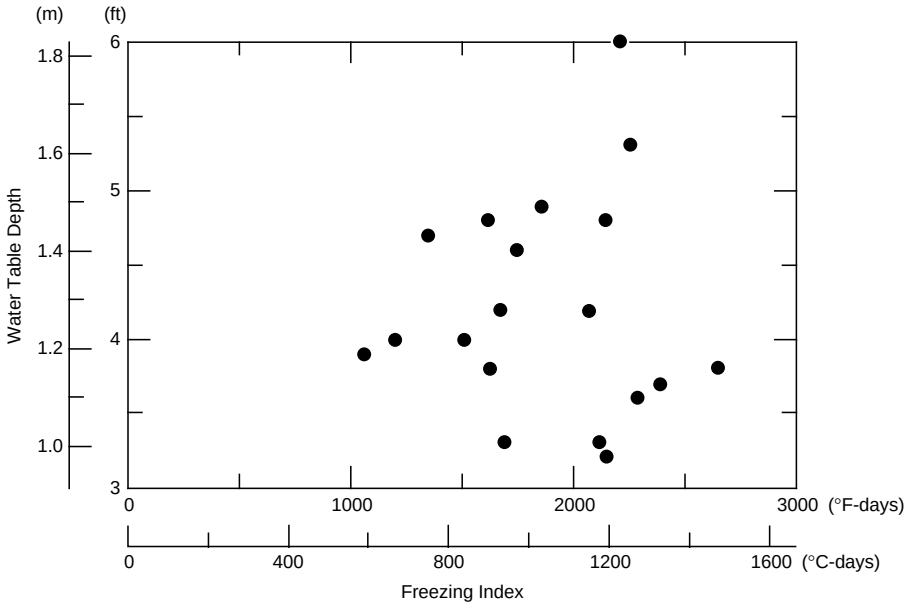

Figure 27. Distribution of freezing indices and water table depths in 21-yr Phase 3 series.

Table 19. Results of 21-yr freezing index/water table series.

					Applications to failure (millions)			
					Horizontal strain		*Vertical strain*	
	Water table depth	*Freezing index*	*Freeze/thaw events in*	*Maximum freeze depth into subgrade*	*Asphalt cracking*		*Subgrade rutting*	
Year	*m (ft)*	*℃ (℉) -days*	*subgrade*	*(cm)*	*CEH*	*AIH-MS11*	*CEV*	*AIV-MS1*
A. Full depth (F4)								
6970	1.5 (4.8)	1191 (2144)	2	91.8	18.20	66.00	0.21	5.38
7071	1.3 (4.2)	1152 (2074)	4	91.8	18.02	52.59	0.34	8.23
7172	1.1 (3.6)	1274 (2294)	2	91.8	15.16	45.02	0.31	7.64
7273	1.2 (4.0)	839 (1510)	2	69.8	18.97	50.69	0.37	7.72
7374	1.3 (4.2)	923 (1661)	2	77.8	17.80	51.48	0.78	10.97
7475	1.4 (4.6)	968 (1743)	3	81.8	17.21	47.93	0.18	5.47
7576	1.3 (4.2)	931 (1675)	3	73.8	16.83	52.26	0.16	4.15
7677	1.6 (5.3)	1256 (2261)	4	107.8	17.92	62.38	0.16	4.87
7778	1.1 (3.7)	1331 (2395)	1	91.8	13.88	60.22	0.10	3.01
7879	1.2 (3.8)	1477 (2658)	3	99.8	17.66	51.36	6.66	17.18
7980	1.2 (3.8)	903 (1625)	5	79.8	16.67	43.10	0.19	5.30
8081	1.2 (4.0)	666 (1199)	3	67.8	17.15	42.63	0.26	7.72
8182	1.8 (6.0)	1227 (2209)	3	107.8	16.29	47.92	0.04	1.44
8283	1.2 (3.9)	589 (1061)	8	63.8	16.73	34.26	0.11	3.71
8384	1.0 (3.3)	1179 (2123)	2	81.8	16.86	48.96	0.12	3.50
8485	1.0 (3.3)	942 (1696)	3	81.8	16.08	44.68	0.15	4.31
8586	1.0 (3.2)	1197 (2154)	2	81.8	17.67	71.27	0.79	11.48
8687	0.9 (3.0)	467 (841)	4	45.8	15.91	33.52	0.48	8.44
8788	1.5 (4.8)	898 (1616)	4	87.8	16.91	48.28	0.34	6.15
8889	1.5 (4.9)	1032 (1858)	4	87.8	17.57	50.53	0.26	7.19
8990	1.4 (4.7)	750 (1350)	7	65.8	16.50	37.45	0.25	6.83

Notes: CEH = Corps of Engineers (horizontal) CEV = Corps of Engineers (vertical)
AIH-MS11 = Asphalt Institute (MS-11) AIV = Asphalt Institute (MS-1)
ND = no damage
Traffic simulated at rate of 660,000 ESAL applications/yr.

Table 19 (cont'd).

Year	Water table depth m (ft)	Freezing index °C (°F) -days	Freeze/thaw events in subgrade	Maximum freeze depth into subgrade (cm)	Applications to failure (millions)			
					Horizontal strain		Vertical strain	
					Asphalt cracking		Subgrade rutting	
					CEH	AIH-MS11	CEV	AIV-MS1
B. Conventional (F3)								
6970	1.5 (4.8)	1191 (2144)	1	13.4	0.46	2.46	0.82	61.97
7071	1.3 (4.2)	1152 (2074)	1	13.4	0.56	2.63	0.47	34.83
7172	1.1 (3.6)	1274 (2294)	1	17.4	0.56	2.53	0.34	26.17
7273	1.2 (4.0)	839 (1510)	0	0	0.49	1.69	ND	ND
7374	1.3 (4.2)	923 (1661)	2	1.4	0.46	2.04	ND	ND
7475	1.4 (4.6)	968 (1743)	1	5.4	0.49	2.61	1.46	120.66
7576	1.3 (4.2)	931 (1675)	1	0	0.55	2.71	ND	ND
7677	1.6 (5.3)	1256 (2261)	1	25.4	0.43	2.18	0.71	58.36
7778	1.1 (3.7)	1331 (2395)	1	13.4	0.49	2.31	0.51	38.69
7879	1.2 (3.8)	1477 (2658)	1	21.4	0.49	2.72	0.36	27.68
7980	1.2 (3.8)	903 (1625)	1	5.4	0.52	1.87	0.44	33.62
8081	1.2 (4.0)	666 (1199)	0	0	0.50	1.50	ND	ND
8182	1.8 (6.0)	1227 (2209)	1	29.4	0.42	2.21	0.46	37.95
8283	1.2 (3.9)	589 (1061)	0	0	0.51	1.34	ND	ND
8384	1.0 (3.3)	1179 (2123)	1	5.4	0.49	1.84	1.18	91.16
8485	1.0 (3.3)	942 (1696)	1	5.4	0.48	1.56	0.98	77.74
8586	1.0 (3.2)	1197 (2154)	1	5.4	0.48	2.70	1.64	ND
8687	0.9 (3.0)	467 (841)	0	0	0.44	1.45	ND	ND
8788	1.5 (4.8)	898 (1616)	1	9.4	0.45	1.85	0.72	58.30
8889	1.5 (4.9)	1032 (1858)	1	9.4	0.53	1.89	0.45	33.69
8990	1.4 (4.7)	750 (1350)	0	0	0.55	1.65	ND	ND

Notes: CEH = Corps of Engineers (horiz.)
CEV = Corps of Engineers (vert.)
AIH-MS11 = Asphalt Institute MS-11
AIV = Asphalt Institute MS-1
ND = no damage
Traffic simulated at rate of 660,000 ESAL applications/yr.

Environmental conditions

The series simulated the 21-yr time period 1969–70 to 1989–90, using a combination of recorded air temperatures and an estimated position of the water table. The simulations started on 1 October of the first year and proceeded for 365 days, using mean daily air temperatures recorded at Buffalo, Minnesota, applied as a step condition for 24-hr periods. The depth to the water table was varied based on the total precipitation accumulated at St. Cloud, Minnesota, during the thaw season prior to the simulated freeze season. An inverse relationship between precipitation and water table depth was applied such that the maximum precipitation produced the shallowest water table at 0.91 m (3 ft) below the surface and the minimum precipitation produced the deepest water table at 1.82 m (6 ft). The water table was held constant throughout the simulation at the depth determined by this relationship. Figure 27 shows the distribution of estimated water table and freeze index for this period.

Results

As in previous simulation series, there was a wide variation in the damage amounts predicted by the different models (Table 19). In general, less damage related to horizontal strain was predicted in the full-depth design than in the conventional design. On the other hand, when all other conditions are constant, there was more damage related to vertical strain in the full-depth design. When frost did not penetrate the subgrade in the conventional design, essentially no vertical strain damage was predicted.

Freeze season characteristics were initially quantified by analyzing the total freezing index, the number of times that frost was predicted to

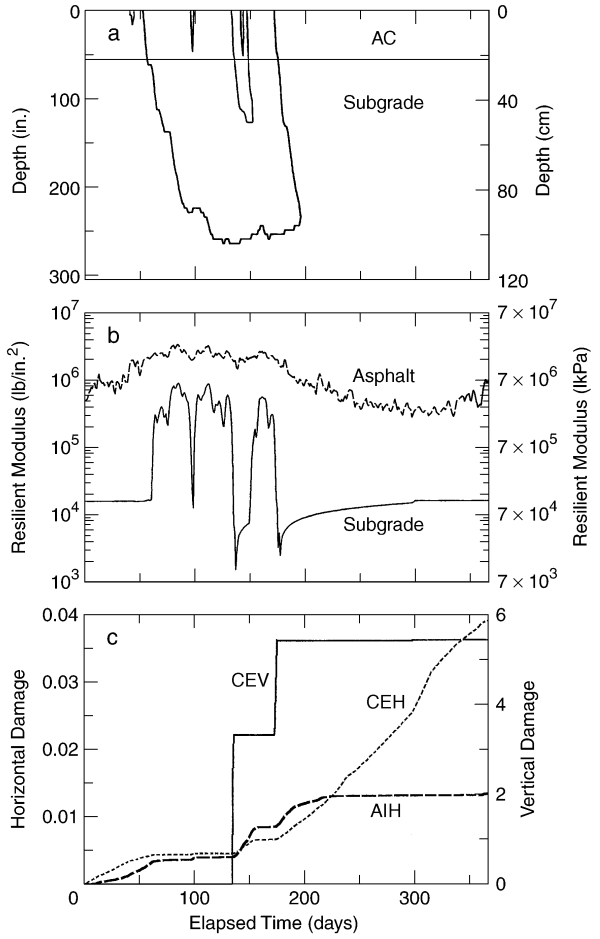

Figure 28. Predicted results from simulation of full-depth section during freeze season 1983–1984, starting on 1 October; a) frost/thaw depth, b) seed resilient modulus passed to NELAPAV, and c) cumulative damage (see Table 19).

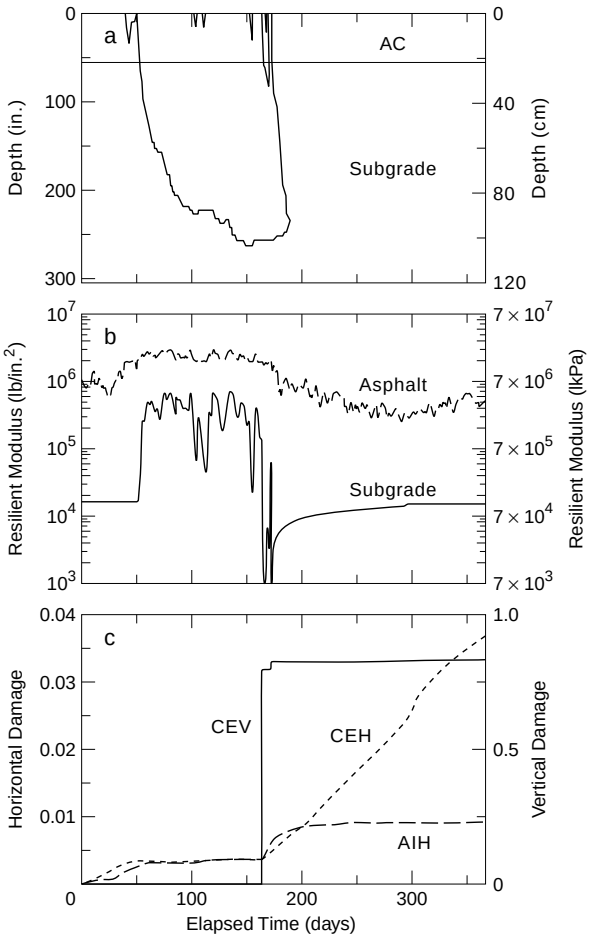

Figure 29. Predicted results from simulation of full-depth section during freeze season 1985–1986, starting on 1 October; a) frost/thaw depth, b) seed resilient modulus passed to NELAPAV, and c) cumulative damage (see Table 19).

enter the subgrade and the maximum depth of frost penetration beneath the top of the subgrade (Table 19). Lower amounts of damage (higher applications to failure) were predicted by the Asphalt Institute horizontal strain model in seasons with higher freezing indices and deeper frost penetration in both the full-depth and conventional cross sections. However, predictions of damage from the other models did not correlate with any of the above parameters.

It was noted that two similarly categorized seasons, 1983–84 and 1985–86, which had nearly identical freezing indexes and water table depths, as well as the same number of freeze thaw events, had diversely different damage predictions in the full-depth section (Table 19a). A large thaw event in the middle of the 1983–1984 freeze season was accompanied by severe weakening of the subgrade both during midwinter and spring thaw, which resulted in a considerable amount of predicted damage (Fig. 28). The 1985–86 year experienced a nearly continuous freeze season with no significant midwinter thaw event (Fig. 29). As a result, the subgrade modulus underwent thaw weakening only during spring thaw in the 1985–86 season, and the corresponding total damage accumulation was much less.

Based on the above observation, we tried a new approach to quantifying the characteristics of the freeze seasons. It involved summing the thawing degree days experienced during the freeze season in two ways. The first was a total from all events,

Table 20. Midwinter season thaw index summations.

Year	Water table depth m (ft)	Freezing index °C(°F)-days	Midwinter thaw index (Total) °C(°F)-days	Midwinter thaw index (> 30 DD) °C(°F)-days
6970	1.5 (4.8)	1191 (2144)	25.5 (45.9)	0.0
7071	1.3 (4.2)	1152 (2074)	41.0 (73.8)	0.0
7172	1.1 (3.6)	1274 (2294)	50.0 (90.0)	19.4 (35.0)
7273	1.2 (4.0)	839 (1510)	21.5 (38.7)	0.0
7374	11.3 (4.2)	923 (1661)	56.0 (100.8)	22.3 (40.1)
7475	1.4 (4.6)	968 (1743)	35.0 (63.0)	14.2 (25.5)
7576	11.3 (4.2)	931 (1675)	67.0 (120.6)	20.7 (37.2)
7677	1.6 (5.3)	1256 (2261)	44.0 (79.2)	0.0
7778	1.1 (3.7)	1331 (2395)	26.5 (47.7)	0.0
7879	1.2 (3.8)	1477 (2658)	52.0 (93.6)	18.0 (32.4
7980	1.2 (3.8)	903 (1625)	32.0 (57.6)	0.0
8081	1.2 (4.0)	666 (1199)	41.0 (73.8)	17.5 (31.5)
8182	1.8 (6.0)	1227 (2209)	31.5 (56.7)	21.9 (39.4)
8283	11.2 (3.9)	589 (1061)	92.5 (166.5)	75.0 (135.0)
8384	1.0 (3.3)	1179 (2123)	40.0 (72.0)	34.7 (62.4)
8485	1.0 (3.3)	942 (1696)	40.0 (72.0)	22.9 (41.2)
8586	1.0 (3.2)	1197 (2154)	29.0 (52.2)	0.0
8687	10.9 (3.0)	467 (841)	65.0 (117.0)	40.1 (72.1)
8788	11.5 (4.8)	898 (1616)	79.0 (142.2)	54.2 (97.6)
8889	1.5 (4.9)	1032 (1858)	49.0 (88.2)	0.0
8990	11.4 (4.7)	750 (1350)	70.5 (126.9)	27.0 (48.6)

and the second was a total from only the thaw events that exceeded 16°C-days (30°F-days) (Table 20). The quantity 16°C-days was chosen based on analysis by Mahoney et al. (1985) indicating that pavements approach their critically weak condition after this amount of thaw has been experienced. Unfortunately, neither of these quantities correlated with predicted damage amounts. Apparently, a more sophisticated index that perhaps combines freeze index, severity of midwinter thaw events, and other parameters is required to correlate with predicted damage.

In analyzing the Phase 3 simulation results, we examined the distribution of predicted damage through the four seasons defined as follows: fall—1 October to start of freeze, winter—freeze season as defined by freezing index, spring—75 days following end of freeze season, summer—remainder of 365-day simulation. The simulations predicted a wide variation in seasonal damage amounts for different years, especially in the vertical strain damage in the conventional cross section (Fig. 30). In years when vertical strain damage was predicted for the conventional cross section, a majority occurred in the spring, while the remainder occurred in the winter (Table 21). Horizontal strain damage in the conventional cross section also occurred mainly in the spring, with additional significant amounts in both the winter and fall, and very small

Table 21. Average percentage of total yearly damage accumulated during four seasons.

Section/model	Accumulated damage (% of total) Fall	Winter	Spring	Summer
Conventional				
AIH	22	31	45	2
AIV	0	40	60	0
CEV	0	42	58	0
Full depth				
AIH	16	51	32	1
AIV	2	44	16	38
CEV	0	80	20	0

Notes:
AIH = Asphalt Institute horizontal (MS-11)
AIV = Asphalt Institute vertical (MS-1)
CEV = Corps of Engineers vertical

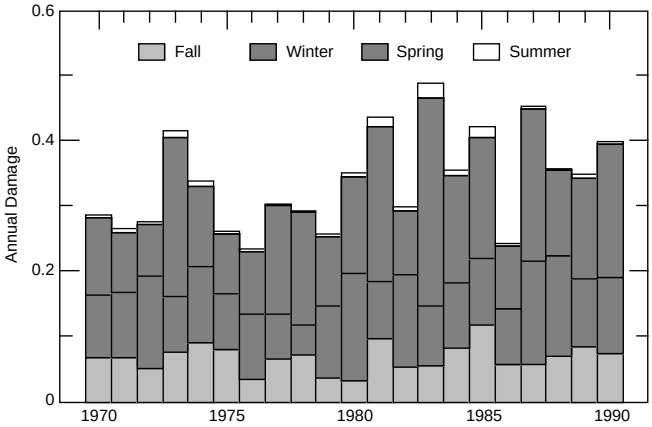

a. Conventional section, Asphalt Institute horizontal strain model MS-11.

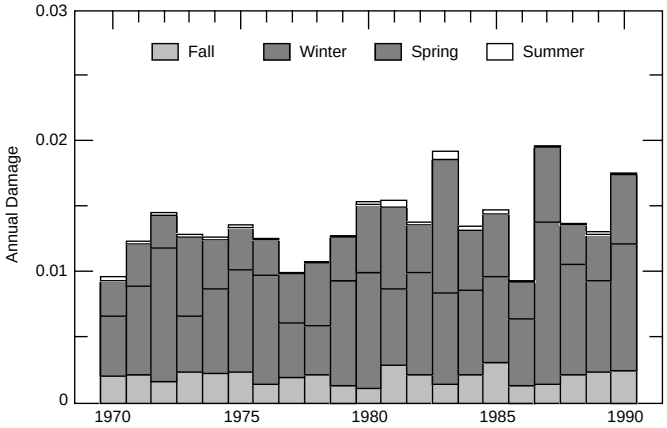

c. Full-depth section, Asphalt Institute horizontal strain model MS-11.

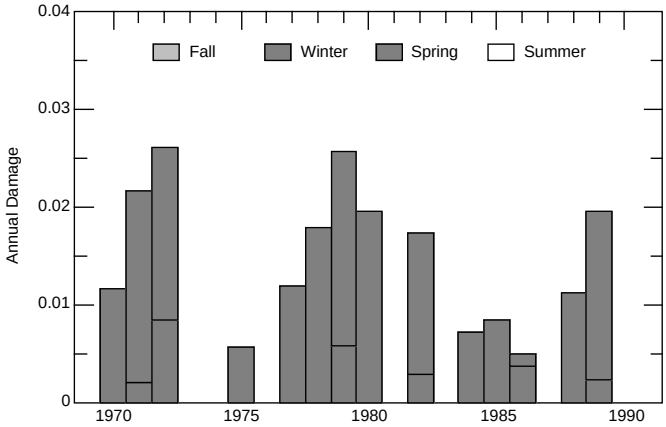

b. Conventional section, Asphalt Institute vertical strain model MS-1.

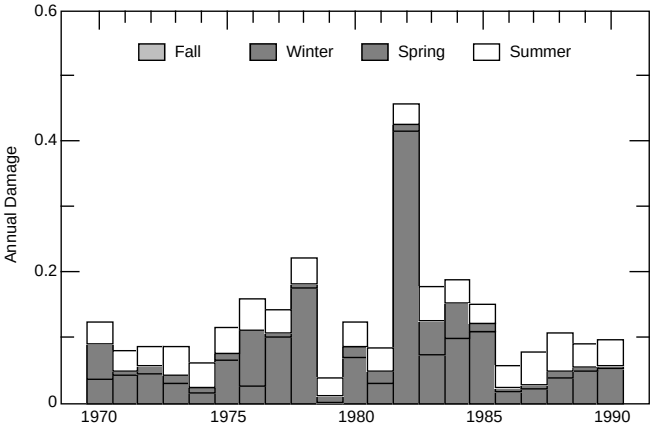

d. Full-depth section, Asphalt Institute vertical strain model MS-1.

Figure 30. Distribution of cumulative damage during seasons.

amounts in the summer. In the full-depth cross section, horizontal strain damage occurred primarily in the winter, with slightly less in the spring, and some additional damage in the fall. Both vertical strain models predicted damage in the full-depth section to occur mainly in the winter, with some in the spring. The Asphalt Institute vertical strain model also predicted additional amounts of summer damage.

DISCUSSION AND RECOMMENDATIONS

The component of this study involving verification of the Mechanistic Pavement Design Procedure results with pavement performance data from Mn/ROAD was not accomplished due to delayed completion of the road.

The Phase 1 modeling series indicated significantly different performance by the different test sections and highly variable results depending on the performance model applied (Table 15). The simulated performance of the test sections was also significantly affected by the subgrade conditions, e.g., density, soil moisture and water table depth. For example, compare the model predictions using the Asphalt Institute MS-1 horizontal strain criteria. For case f4w6, the full-depth 5-yr section with the 1206 subgrade in its high density condition, the model predicts 28,585,000 applications to failure. In case f4w6ld, the same test section with a low density value for the 1206 subgrade, the model predicts 1,905,000 applica-

tions to failure. And finally, in case f4w6ss, with the 1232 subgrade that produced lower resilient modulus values in lab tests, failure is predicted after only 72,000 applications, or in less than one year.

After the Phase 1 simulations were complete, the resilient modulus data from the 1206 subgrade were reviewed. A calibration error of unknown magnitude was discovered in the resilient modulus equipment used to measure the unfrozen modulus on that material. Modulus testing of the 1206 subgrade in the frozen condition and all testing on the other materials were conducted on a different machine, which passed its calibration checks. Comparing frozen and unfrozen resilient modulus test results from the 1206 subgrade with those from other materials tested (Fig. 14) indicates that the unfrozen M_r values for the 1206 subgrade may be about an order of magnitude too high. A lower M_r for the 1206 subgrade would have resulted in earlier failures than computed in this report where the 1206 optimum density subgrade was used.

We are currently investigating the unfrozen 1206 subgrade results and will include findings and revised performance predictions in Berg (in prep).

It is obviously extremely important to use the representative subgrade conditions in the design simulations. Results are consistent with observations from in-service pavements; e.g., weak areas fail much more rapidly than strong ones and high water tables cause failures before similar pavements constructed over lower water tables. Both the "1206" and "1232" subgrade samples were obtained from the test site and were located less than one-half mile apart, yet their tested behavior was quite different. It is hoped that the actual subgrade will perform more like the "1206" subgrade than the "1232" material.

Another important aspect governing the results of the Mechanistic Pavement Design Procedure is the method used to calculate the asphalt concrete resilient modulus. The use of the Schmidt model, which produces extremely low summer season resilient moduli, partially accounts for the short lifespans predicted in the Phase 1 modeling series. Replacement with the Ullidtz model at temperatures above 1°C in the Phase 2A modeling series increased the predicted lifespans of the sections when judged by the horizontal strain criteria (Table 17).

Results from the Phase 2A series that used the Ullidtz model for asphalt modulus calculations and a recovered summer subgrade modulus of 1.03 $\times 10^5$ kPa (15,000 lb/in.^{2}), a close approximation of the value back-calculated from FWD measurements on subgrade during fall 1991, yield performance predictions that are as "fine-tuned" as possible, so far (Table 17 "Ull-15K"). When these Mechanistic Pavement Design Procedure predictions are compared with the designed failure at 3,300,000 applications for the 5-yr sections and 6,600,000 applications for the 10-yr sections, the following statements can be made:

1. Predictions for the full depth sections, both 5 and 10 yr, indicate that they will not fail prematurely from asphalt cracking, but two of the three criteria for subgrade rutting indicate early failure.

2. Conventional sections are predicted not to fail due to subgrade rutting; however, sections with more frost-susceptible bases are predicted to fail because of asphalt cracking relatively early in their design life, and sections with non-frost-susceptible bases are predicted to fail towards the end of their design life.

By modeling 21 years of environmental conditions in the Phase 3 series, we were hoping to identify the characteristics of a winter that could be used for design purposes. The results were complex and a relation between predicted failure and characteristics of freeze seasons was elusive, at best.

It is recommended that funding be located for the following studies:

- The class 4 special and class 5 special base materials should receive the full complement of laboratory tests so that simulations may be run using properties of actual materials from the site rather those of substitute materials.
- Once performance data are received from Mn/ROAD, predicted and measured values of moisture, temperature, strains and failure times should be compared to complete the verification component of the study.
- Use performance data from Mn/ROAD to revise, refine or develop new damage models for rutting and fatigue cracking.
- Use performance data from Mn/ROAD to refine or develop a new model for the change of the asphalt modulus with temperature.
- Use data from falling weight deflectometer

tests on Mn/ROAD to estimate pavement performance on an annual basis.

- The Mechanistic Pavement Design Procedure should be used to estimate performance of all of the test sections. This study evaluated less than one-half of the sections.

CONCLUSIONS*

The range of values produced for the various scenarios is, as noted, extremely wide. This leads to the conclusion that mechanistic design in its present stage, while a powerful predictor of changes in pavement response with changes in loads or moduli, is at present an uncertain predictor of pavement performance. Data and analyses from Mn/ROAD are crucial to improving that current uncertain state of performance prediction.

LITERATURE CITED

The Asphalt Institute (1982) Research and development of the Asphalt Institute's thickness design manual (MS-1), Ninth Edition. College Park, Maryland. Research Report No. 82-2.

R. Berg (in prep.) Resilient modulus testing of materials from Mn/ROAD, Phase 2. USA Cold Regions Research and Engineering Laboratory, Special Report.

Berg, R.L., S.R. Bigl, J. Stark and G. Durell (1996) Resilient modulus testing of materials from Mn/ROAD, Phase 1. USA Cold Regions Research and Engineering Laboratory, Special Report 96-19, Mn/DOT Report 96-21.

Berg, R.L., G.L. Guymon and T.C. Johnson (1980) Mathematical model to correlate frost heave of pavements with laboratory predictions. USA Cold Regions Research and Engineering Laboratory, CRREL Report 80-10.

Bigl, S.R. and R.L. Berg (1996a) Testing of materials from the Minnesota Cold Regions Pavement Research Test Facility. USA Cold Regions Research and Engineering Laboratory, Special Report 96-20, Mn/DOT Report 96-24.

Bigl, S.R. and R.L. Berg (1996b) Modeling of Mn/ROAD test sections with the CRREL mechanistic pavement design procedure. USA Cold Regions Research and Engineering Laboratory, Special Report 96-21, Mn/DOT Report 96-22.

Bush, A. (1980) Non-destructive testing for light aircraft pavements. USAE Waterways Experiment Station, Vicksburg, Mississippi (sponsored by the Federal Aviation Administration).

Chamberlain, E.J. (1987) A freeze thaw test to determine the frost susceptibility of soils. USA Cold Regions Research and Engineering Laboratory, special Report 87-1.

Chamberlain, E.J., T.C. Johnson, R.L. Berg and D.M. Cole (in prep.) Prediction of pavement behavior under loading during freezing and thawing. USA Cold Regions Research and Engineering Laboratory, CRREL Report.

Chou, Y.T (1989) Development of failure criteria of rigid pavement thickness requirements for military roads and streets, elastic layered method. USAE Waterways Experiment Station, Vicksburg, Mississippi, Miscellaneous Paper GL-89-9.

Cole, D., D. Bently, G. Durell and T. Johnson (1986) Resilient modulus of freeze-thaw affected granular soils for pavement design and evaluation, Part 1. Laboratory tests on soils from Winchendon, Massachusetts, test sections. USA Cold Regions Research and Engineering Laboratory, CRREL Report 86-4.

Cole, D., D. Bently, G. Durell and T. Johnson (1987) Resilient modulus of freeze-thaw affected granular soils for pavement design and evaluation, Part 3. Laboratory tests on soils from Albany county airport. USA Cold Regions Research and Engineering Laboratory, CRREL Report 87-2.

Coetzee, N.F. and B.G. Connor (1990) Fatigue characteristics of Alaskan pavement mixes. Transportation Research Record No. 1269, Transportation Research Board, National Research Council, Washington D.C., p.168–175.

Gardner, W.R. (1958) Some steady-state solutions of the unsaturated flow equation with application to evaporation from a water table. *Soil Science*, **88**: 228–232.

Guymon, G.L., R.L. Berg and T.V. Hromadka (1993) Mathematical model of frost heave and thaw settlement in pavements. USA Cold Regions Research and Engineering Laboratory, CRREL Report 93-2.

Ingersoll, J. (1981) Method for coincidentally determining soil hydraulic conductivity and mois-

* This was written by G. Cochran, Mn/ROAD, pers. comm. 1994.

ture retention characteristics. USA Cold Regions Research and Engineering Laboratory, Special Report 81-2.

Irwin, L. and D. Speck (1986) NELAPAV user's guide. Cornell University, Ithaca, New York, Cornell University Local Road Program Report No. 86-1

Mahoney, J.P., J.A. Lary, J. Sharma and N. Jackson (1985) Investigation of seasonal load restrictions in Washington state. Transportation Research Record 1043, TRB, National Research Council, Washington D.C., p. 58–67.

Schmidt, R.J. (1975) Use of ASTM tests to predict low temperature stiffness of asphalt mixes. Transportation Research Record 544, TRB, National Research Council, Washington, D.C. p. 35–45.

Tice, A.R., J.L. Oliphant, Y. Nakano and T.F. Jenkins (1982) Relationship between the ice and unfrozen water phases in frozen soil as determined by pulsed nuclear magnetic resonance and physical absorption data. USA Cold Regions Research and Engineering Laboratory, CRREL Report 82-15.

Ullidtz, P. (1987) Pavement analysis. In *Developments in Civil Engineering*, Vol. 19. Amsterdam: Elsevier Science Publishers.

U.S. Army (1987) Flexible pavement design for airfields (layered elastic method). Department of the Army, Washington, D.C. Draft Technical Manual TM 5-825-2-1.

U.S. Army (1988) Pavement design for roads, streets, and open storage areas, elastic layered method. Department of the Army, Washington, D.C. Technical Manual TM 5-800-09.

U.S. Army (1990) Rigid pavements for airfields other than Army (layered elastic method). Department of the Army,Washington, D.C. Technical Manual TM 5-824-2-1.

Witczak, M. (1972) Design of full depth airfield pavements. *Proceedings, Third International Conference on the Structural Design of Asphalt Pavements.* London, England, Vol. I, p. 450–467.

Yang, W. (1988) Mechanistic analysis of nondestructive pavement deflection data. Doctorate dissertation, Cornell University, Ithaca, New York (unpublished).

REPORT DOCUMENTATION PAGE

Form Approved
OMB No. 0704-0188

1. AGENCY USE ONLY (Leave blank)	2. REPORT DATE	3. REPORT TYPE AND DATES COVERED
	September 1996	Final Report June 1988–October 1994

4. TITLE AND SUBTITLE

Material Testing and Initial Pavement Design Modeling: Minnesota Road Research Project

5. FUNDING NUMBERS

CPAR Project
Agreement No. 64632
Task Order No. 1

6. AUTHORS

Susan R. Bigl and Richard L. Berg

7. PERFORMING ORGANIZATION NAME(S) AND ADDRESS(ES)

U.S. Army Cold Regions Research and Engineering Laboratory
72 Lyme Road
Hanover, New Hampshire 03755-1290

8. PERFORMING ORGANIZATION REPORT NUMBER

CRREL Report 96-14

9. SPONSORING/MONITORING AGENCY NAME(S) AND ADDRESS(ES)

Minnesota Department of Transportation
395 John Ireland Boulevard Mail Stop 330
St. Paul, Minnesota 55155

10. SPONSORING/MONITORING AGENCY REPORT NUMBER

MN/RC-96/23

11. SUPPLEMENTARY NOTES

For conversion of SI units to non-SI units of measurement consult ASTM Standard E380-93, *Standard Practice for Use of the International System of Units*, published by the American Society for Testing and Materials, 1916 Race St., Philadelphia, Pa. 19103.

12a. DISTRIBUTION/AVAILABILITY STATEMENT

Approved for public release; distribution is unlimited.

Available from NTIS, Springfield, Virginia 22161

12b. DISTRIBUTION CODE

13. ABSTRACT (*Maximum 200 words*)

Between January 1990 and December 1994, a study verified and applied a Corps of Engineers-developed mechanistic design and evaluation method for pavements in seasonal frost areas as part of a Construction Productivity Advancement Research (CPAR) project between the Minnesota Department of Transportation (Mn/DOT) and the U.S. Army Cold Regions Research and Engineering Laboratory (CRREL). The study involved four primary components. Mn/DOT constructed a full scale pavement test facility adjacent to Interstate 94, referred to as the Minnesota Road Research Project (Mn/ROAD). CRREL performed extensive laboratory tests on the base and subgrade materials from Mn/ROAD to characterize them and their behavior under seasonal frost conditions. Laboratory tests provided the input parameters necessary for the study's third component, modeling with the CRREL Mechanistic Pavement Design and Evaluation Procedure. The modeling effort was conducted in three phases, which investigated the effects of freeze season characteristics, water table position, asphalt model and subgrade characteristics on the predicted performance of selected Mn/ROAD test sections. Delays in construction on the Mn/ROAD facility prevented the completion of the study's fourth component—using performance data from Mn/ROAD to validate the mechanistic pavement design and evaluation procedure. The report details results from the other three components.

14. SUBJECT TERMS

Mechanistic pavement design and evaluation procedure
Construction Productivity Advancement Research (CPAR)
Freeze season characteristics
Pavement performance

15. NUMBER OF PAGES
56

16. PRICE CODE

17. SECURITY CLASSIFICATION OF REPORT	18. SECURITY CLASSIFICATION OF THIS PAGE	19. SECURITY CLASSIFICATION OF ABSTRACT	20. LIMITATION OF ABSTRACT
UNCLASSIFIED	UNCLASSIFIED	UNCLASSIFIED	UL